

# Phenomenological Analysis of $pp$ and $\bar{p}p$ Elastic Scattering Based on Theoretical Bounds in High-Energy Physics

S. D. Campos\*

*Universidade Federal de São Carlos, campus de Sorocaba, 18052-780, Sorocaba, SP, Brazil.*

V. A. Okorokov†

*National Research Nuclear University "MEPhI", Kashirskoe Shosse 31, 115409 Moscow, Russia*

Considering the Froissart-Martin bound, Jin-Martin-Cornille bound and the optical theorem, we propose a novel parametrization for the total cross-section of proton-proton and antiproton-proton elastic scattering data. Using derivative dispersion relations we obtain the real part of the elastic scattering amplitude and thus the  $\rho$  parameter. Simultaneous fits to  $\sigma_{\text{tot}}$  and  $\rho$  are performed allowing very good statistical descriptions of the available data. Furthermore, predictions to  $\sigma_{\text{tot}}$  and  $\rho$  at energies not used in the fit procedures are presented. For  $\sigma_{\text{tot}}$  we obtain predictions at RHIC, LHC and future HC energies.

PACS numbers: 13.85.Dz; 13.85.-t

## I. INTRODUCTION

Nowadays, the study of high energy scattering is one of the most exciting topics in physics, and we have, as far we know, the exact theory of strong interactions, Quantum Chromodynamics (QCD), which can describe, based on the perturbative calculation scheme, the hadron-hadron interactions at short distances. However, interactions at large distances (near forward scattering) cannot be calculated even within perturbative approaches. Proton-proton ( $pp$ ) and antiproton-proton ( $\bar{p}p$ ) elastic scattering are the simplest processes not yet explained in terms of a pure QCD description. The absence of such a description allows empirical analyses based on models [1–14] or almost-independent models (some experimental data set possess theoretical bias) [15] whose main goal is to fit the available experimental data extracting useful information, contributing to the development of novel computational schemes. Several phenomenological models for high energy scattering are based on general principles of the Axiomatic Quantum Field Theory (AQFT), such as unitarity and crossing-symmetry, and on derived results as analyticity, and have proven to be successful in understanding or predicting the behavior of the hadronic scattering amplitude.

Empirical parametrization for the total cross-section, differential cross-section, slope of the differential cross-section and others physical quantities have widely been used as a source of phenomenological model-independent indications of the experimental data behavior. These approaches must be seen as a first step or attempt toward a formally rigorous phenomenological model-independent description of high energy elastic hadron scattering, embodying a predictive character. Moreover, important high energy theorems and bounds have been demonstrated in the last decades, providing rigorous formal constraints in the region of asymptotic energies, which cannot be disregarded in any reliable formalism, mainly related with phenomenological model-independent approaches. Of course, we must keep in mind that AQFT is a mathematical framework for the treatment and interpretation of relativistic quantum field theories and, in general, not all formal results based on AQFT results are satisfied by QCD.

In this work, we present a novel parametrization based on formal high energy bounds taken from AQFT for the total cross-section of the elastic scattering amplitude. Specifically, we introduce a novel analytical parametrization for the total cross-section, inferred assuming some rigorous high energy bounds. The real part of the scattering amplitude is analytically evaluated through derivative dispersion relation. The crossing symmetry relates particle-particle and particle-antiparticle amplitudes. Fits to  $pp$  and  $\bar{p}p$  total cross-section,  $\rho$  parameter are performed and may lead to a predictive and phenomenological model-independent approach, able to describe quite well the bulk of the experimental data. Furthermore, we present some predictions for the total cross-section for the LHC run at  $\sqrt{s} = 7.0, 10,$  and  $14$  TeV, for the future HC at  $\sqrt{s} = 50, 100, 200$  and  $500$  TeV and for the RHIC experiment at  $\sqrt{s} = 200$  and  $500$  GeV. It is important to stress that the parametrization proposed here allows us to obtain, under some physical conditions, the whole scattering function (beyond the forward direction). We intend to show these analyses elsewhere.

---

\*Electronic address: sergiode@ufscar.br

†Electronic address: okorokov@bnl.gov; VAOkorokov@mephi.ru

The paper is organized as follows. In section II, the Froissart-Martin bound [16, 17], Jin-Martin-Cornille bound [18, 19] and the optical theorem are used to propose a novel parameterization for  $pp$  and  $\bar{p}p$  total cross-section and  $\rho$  parameter using only four fit parameters to each scattering reaction. In section III we explicitly obtain the real part of the forward elastic scattering amplitude and the  $\rho$  parameter. In section IV we show the individual fit results for  $\sigma_{\text{tot}}$  and  $\rho$ . In section V we show the simultaneous fit results for  $\sigma_{\text{tot}}$  and  $\rho$ . Section VI presents a possible interpretation for the effective physical mechanism of this model comparing it with some models present in the literature. In section VII we present our Final Remarks with some criticism.

## II. TOTAL CROSS-SECTION

The total cross-section is one of the most important physical observable in the elastic scattering. Its energy dependence has been a focus of intense theoretical interest since the establishment of QCD as *the* theory of strong interactions. However, at high energies there is no description based only on pure QCD formalism and the use of models with free fit parameters is the usual way to study  $pp$  and  $\bar{p}p$  elastic scattering. In this section one obtains a novel parametrization for the total cross-section based on well-established results taken from AQFT.

We start considering the scattering amplitude  $F(s, q^2)$  expressed as a function of two Mandelstam variables in the center-of-mass system, usually the energy squared  $s$  and the momentum transfer squared  $t = -q^2$ . We can write  $F(s, q^2)$  in terms of its real and imaginary parts as

$$F(s, q^2) = \text{Re}F(s, q^2) + i\text{Im}F(s, q^2),$$

where the imaginary part of  $F$  represents the absorption in the scattering process and usually is related to the real part by dispersion relation (integral or derivative) that analytically connects  $pp$  and  $\bar{p}p$  elastic scattering through crossing property. Therefore, if we know  $\text{Im}F(s, q^2)$ , then we are able to compute analytically the whole scattering amplitude (at  $q^2 = 0$ ).

The main goal of this section is to propose  $pp$  and  $\bar{p}p$  total cross-section considering high energy bounds from formal results of the AQFT. A fundamental result derived from unitarity and analyticity asserts that high energy total cross-sections for the hadronic forward elastic scattering (at  $q^2 = 0$ ) should be bounded according to Froissart-Martin bound [16, 17]

$$\sigma_{\text{tot}} \leq \frac{\pi}{m_\pi^2} \ln^2(s/s_0), \quad (1)$$

where  $\sigma_{\text{tot}} = \sigma_{\text{tot}}(s)$  is the total cross-section of  $pp$  and  $\bar{p}p$  and  $s_0$  is some energy initial value. Henceforth, we shall adopt  $s_0 = 1 \text{ GeV}^2$ . This bound refers to an energy dependence of the total cross-section rising no more rapidly than  $\ln^2 s$ . As a remark, unfortunately, at present day we cannot be unambiguously discriminate between asymptotic fits of  $\ln s$  and  $\ln^2 s$  using high energy data [20–22].

On the other hand, Cornille [19] improving the result of Jin and Martin [18] proved the asymptotic lower bound

$$\sigma_{\text{tot}} \geq \frac{\delta}{s^6}. \quad (2)$$

Using both formal results (1) and (2) we propose the following parametrization for the total cross-section

$$\sigma_{\text{tot}}^{pp} = \frac{\delta}{s^{6+\gamma}} + \frac{\pi\beta}{\sqrt{2}s^\alpha m_\pi^2} \ln^2 s, \quad (3)$$

$$\sigma_{\text{tot}}^{\bar{p}p} = \frac{\bar{\delta}}{s^{6+\bar{\gamma}}} + \frac{\pi\bar{\beta}}{\sqrt{2}s^{\bar{\alpha}} m_\pi^2} \ln^2 s. \quad (4)$$

The first term in the right hand side of (3) and (4) will be responsible for the description of the data at low energies. Therefore,  $\delta$  and  $\bar{\delta}$ ,  $\gamma$  and  $\bar{\gamma}$  will be slightly different and at very high energies both terms must vanish. Yet,  $\alpha$  and  $\bar{\alpha}$  also has a role at low energies allowing a more accurate description of the low energy data. Nevertheless, the second term in the right hand side of both parameterizations will be the leading one at high energies. Using the Pomeranchuk theorem,  $\beta$  and  $\bar{\beta}$ ,  $\alpha$  and  $\bar{\alpha}$  must tend to the same numerical value.

As seen above, in the fitting process for the total cross-section data we expect  $\alpha \rightarrow 0$  as well as  $\gamma \rightarrow -6$ , and therefore,  $s^{6+\gamma} \rightarrow 1$  and  $s^\alpha \rightarrow 1$  indicating the saturation of the Froissart-Martin bound. However, at the present day energy scale, we do not expect  $\alpha = 0$  and so even really small values of  $\alpha$  will give a slow increase with  $s$  for

the total cross-section when compared with the "full" Froissart-Martin bound. One consider here the  $\alpha$ -parameter as some kind of "correction term" in the Froissart-Martin bound at low energies and it may represents some physical mechanisms that avoid the total cross-section saturation.

As mentioned above,  $\alpha$  may be treated as a correction in the Froissart-Martin bound at low energy. However, at (finite) high energies all the second term in the right hand side of (3) and (4) will behave as some power of  $s$

$$\frac{\pi\beta}{\sqrt{2}s^\alpha m_\pi^2} \ln^2 s \rightarrow cs^p. \quad (5)$$

where  $c$  is a convenient constant and  $p$  the effective index.

In order to apply the results obtained above to analyze the total cross-section data, we notice the important result assuring that if the Froissart-Martin is reached then the difference between  $pp$  and  $\bar{p}p$  total cross-section goes as [23–25]

$$\Delta\sigma_{\text{tot}} = \sigma_{\text{tot}}^{pp} - \sigma_{\text{tot}}^{\bar{p}p} \leq c \frac{\sigma_{\text{tot}}^{pp} + \sigma_{\text{tot}}^{\bar{p}p}}{\ln s},$$

which means that the difference can increases at most as  $\ln s$  and even in this case,

$$\frac{\sigma_{\text{tot}}^{pp}}{\sigma_{\text{tot}}^{\bar{p}p}} \rightarrow 1,$$

as  $s \rightarrow \infty$ . This is the revised version of the Pomeranchuk theorem and in order to obey this formal result, we must impose the following constraints

$$\delta = \bar{\delta}, \quad \gamma = \bar{\gamma}, \quad \alpha = \bar{\alpha}, \quad \beta = \bar{\beta}. \quad (6)$$

Nevertheless, the energies achieved in the collision processes allow to release these constraints and therefore, as a first step, we adopt in the fitting procedure four independent parameters to  $pp$  and four to  $\bar{p}p$ .

### III. REAL PART OF THE ELASTIC SCATTERING AMPLITUDE AND $\rho$ PARAMETER

In this section, we shall obtain the real part of the forward elastic scattering amplitude. In particular, we obtain  $\rho(s)$ , the ratio of the real to imaginary part of the forward scattering amplitude in the high energy domain.

The optical theorem connects the total cross-section to imaginary part of the elastic scattering at  $q^2 = 0$ . On the other hand, since the imaginary part of the elastic scattering amplitude may be connected to the real part using dispersion relation one concludes that forward elastic scattering amplitude possess the same free parameters, except for the free-parameters coming from the subtraction terms of the dispersion relation, of the total cross-section. Connections between real and imaginary parts of the forward scattering amplitude have been widely investigated by dispersion relation in both integral and derivative forms (we use here the derivative form). Several papers have been devoted to calculations of the real parts of the  $pp$  and  $\bar{p}p$  forward scattering amplitude, using a wide variety of dispersion relations and different representations for the energy dependence of the imaginary part of the scattering amplitude at  $q^2 = 0$ . Here, to obtain the real part of the elastic scattering amplitude, we use the approach adopted in [15, 26]. We define two auxiliary functions (crossing between  $pp$  and  $\bar{p}p$ )

$$\frac{\text{Im}f_{\pm}}{s} = \frac{1}{2} \left[ \frac{\text{Im}F_{pp}}{s} \pm \frac{\text{Im}F_{\bar{p}p}}{s} \right],$$

and relate these functions with the elastic scattering amplitude  $F_{pp/\bar{p}p} = f_+ \pm f_-$ , where  $f_+ = \text{Re}f_+ + i\text{Im}f_+$  and  $f_- = \text{Re}f_- + i\text{Im}f_-$  and  $f_{\pm}$  are convenient amplitudes. In the forward direction, the derivative dispersion relation for even (+) and odd (-) amplitudes are expressed in terms of a tangent operator and in the case of one subtraction (equal to two subtractions in the even case) they are given by [27]

$$\frac{\text{Re}f_+(s,0)}{s} = \frac{k}{s} + \tan \left[ \frac{\pi}{2} \frac{d}{d \ln s} \right] \frac{\text{Im}f_+(s,0)}{s},$$

$$\frac{\text{Re}f_-(s,0)}{s} = \tan \left[ \frac{\pi}{2} \left( 1 + \frac{d}{d \ln s} \right) \right] \frac{\text{Im}f_-(s,0)}{s}.$$

On the other hand, Bronzan, Kane and Sukhatme [28] obtained derivative dispersion relations (without subtraction constant) using an integration parameter  $\nu$ . This parameter was used as free fit parameter or considered as constant over years [27].

$$\frac{\text{Re}f_+(s, 0)}{s^\nu} = \tan \left[ \frac{\pi}{2} \left( \nu - 1 + \frac{d}{d \ln s} \right) \right] \frac{\text{Im}f_+(s, 0)}{s^\nu},$$

$$\frac{\text{Re}f_-(s, 0)}{s^\nu} = \tan \left[ \frac{\pi}{2} \left( \nu + \frac{d}{d \ln s} \right) \right] \frac{\text{Im}f_-(s, 0)}{s^\nu},$$

and Kang and Nicolescu [29] obtained derivative dispersion relations without  $\nu$  parameter (without subtraction constant) and

$$\frac{\text{Re}f_+(s, 0)}{s} = \left[ \frac{\pi}{2} \frac{d}{d \ln s} + \frac{1}{3} \left( \frac{\pi}{2} \frac{d}{d \ln s} \right)^3 + \frac{2}{5} \left( \frac{\pi}{2} \frac{d}{d \ln s} \right)^5 + \dots \right] \frac{\text{Im}f_+(s, 0)}{s},$$

$$\frac{\text{Re}f_-(s, 0)}{s} = -\frac{2}{\pi} \int \left[ 1 - \left( \frac{\pi}{2} \frac{d}{d \ln s} \right)^2 - \frac{1}{45} \left( \frac{\pi}{2} \frac{d}{d \ln s} \right)^4 - \dots \right] \frac{\text{Im}f_-(s, 0)}{s} d \ln s.$$

Ávila and Menon [27] obtained the same result as Bronzan, Kane and Sukhatme without  $\nu$  parameter, which is equivalent to consider  $\nu = 1$  in Bronzan, Kane and Sukhatme results. The odd case of Kang and Nicolescu can be obtained from Ávila and Menon expressions replacing  $\tan \left[ \frac{\pi}{2} \left( 1 + \frac{d}{d \ln s} \right) \right] \rightarrow -\cot \left[ \frac{\pi}{2} \frac{d}{d \ln s} \right]$  and expanding the series around the origin in Ávila and Menon derivative dispersion relations [27]. Furthermore, results of Ávila and Menon are equivalent to Bronzan, Kane and Sukhatme considering the particular case  $\nu = 1$ .

It is important to stress that replacement  $\tan \left[ \frac{\pi}{2} \left( 1 + \frac{d}{d \ln s} \right) \right] \rightarrow -\cot \left[ \frac{\pi}{2} \frac{d}{d \ln s} \right]$  may present some theoretical flow. As known, the first term of the  $\cot(x)$  expansion presents the application of the inverse of the derivative operator. Mathematically speaking, let  $\Pi$  a linear operator. Its inverse,  $\Pi^{-1}$ , is by definition ( $H(x)$  is a non-zero analytic function)

$$\Pi[\Pi^{-1}H(x)] = \Pi^{-1}[\Pi H(x)] = H(x).$$

Furthermore,  $\Pi^{-1}$  is also linear [30]. Of course, we consider  $x$  as an element of a linear space with a well-defined norm. In the context of the operatorial algebra, there exist  $\Pi^{-1}$  if and only if to  $m > 0$

$$m\|H(x)\| \leq \|\Pi H(x)\|. \quad (7)$$

To the specific case where  $\Pi \equiv \frac{d}{d \ln s}$  is always possible obtain  $m$  to satisfy the above result. However, we must take in to account the possible divergence result, i.e.,

$$\frac{d}{d \ln s} H(s) = 0,$$

and therefore  $1/(d/d \ln s) \rightarrow \infty$ . The above result may be viewed as a possible limitation to the functional form of the imaginary part of the forward amplitude: it cannot be constant in  $d/d \ln s$ . Of course, this result is valid only if the formal procedure presented above is correct.

It has also been demonstrated by Fischer and Kolář [31–33] that at high energies the above even tangent operator can be replaced by its first order expansion. The odd representation also can be replaced by its first term [33] by using the notation of Kang and Nicolescu. However, Ávila and Menon and Kang and Nicolescu representations are equivalent by the transformation showed above. Therefore, we retain here, for the sake of simplicity, only the first term of tangent series expansion in the Ávila and Menon representation for both even and odd derivative dispersion relations.

$$\frac{\text{Re}f_+(s, 0)}{s} = \frac{k}{s} + \frac{\pi}{2} \frac{d}{d \ln s} \frac{\text{Im}f_+(s, 0)}{s},$$

$$\frac{\text{Re}f_-(s, 0)}{s} = \frac{\pi}{2} \left( 1 + \frac{d}{d \ln s} \right) \frac{\text{Im}f_-(s, 0)}{s}.$$

This approach was recently used presenting good statistical results [15]. Of course, other terms of the tangent series expansion could be considered as perturbations of the first (leading) term.

The real part of the scattering amplitude is given by

$$\frac{\text{Re}F_{pp/\bar{p}p}(s, 0)}{s} = \frac{\text{Re}f_+(s, 0)}{s} \pm \frac{\text{Re}f_-(s, 0)}{s}.$$

The most general versions of local quantum field theory lead to proving dispersion relation and, more generally, analyticity properties in two variables in a rather large domain, if one makes use of the positivity properties of the absorptive part of the scattering amplitude. Empirically, over many years, dispersion relation had always been consistent with measured data for energies reached by fixed target machines (e.g. pion nucleon scattering) or colliders (ISR and Sp $\bar{p}$ S colliders). Therefore, considering the above formalism we obtain ( $pp$  and  $\bar{p}p$ )

$$\frac{\text{Re}F_{pp}(s, 0)}{s} = \frac{k}{s} + \frac{\pi}{2} \left[ -\frac{\delta(6+\gamma)}{s^{6+\gamma}} + \frac{\pi\beta\sqrt{2}}{m_\pi^2 s^\alpha} \left( \ln s - \frac{\alpha \ln^2 s}{2} \right) \right] + \frac{\pi}{4} [\sigma_{\text{tot}}^{pp} - \sigma_{\text{tot}}^{\bar{p}p}], \quad (8)$$

$$\frac{\text{Re}F_{\bar{p}p}(s, 0)}{s} = \frac{k}{s} + \frac{\pi}{2} \left[ -\frac{\bar{\delta}(6+\bar{\gamma})}{s^{6+\bar{\gamma}}} + \frac{\pi\bar{\beta}\sqrt{2}}{m_\pi^2 s^{\bar{\alpha}}} \left( \ln s - \frac{\bar{\alpha} \ln^2 s}{2} \right) \right] - \frac{\pi}{4} [\sigma_{\text{tot}}^{pp} - \sigma_{\text{tot}}^{\bar{p}p}], \quad (9)$$

where the crossing property allows the simultaneous analysis to  $pp$  and  $\bar{p}p$  scattering amplitude. Notice that  $pp$  and  $\bar{p}p$  forward scattering amplitudes interact with each other by means the crossing property.

At high energies is expected that the imaginary part of the elastic scattering amplitude dominate the real part, i.e., the absorptive part will represents the whole scattering amplitude. Therefore, a simple measure of how fast the imaginary part increases is given by  $\rho$ , the ratio of the real to imaginary part of the forward scattering amplitude in the high energy domain

$$\rho(s) = \frac{\text{Re}F(s, 0)}{\text{Im}F(s, 0)},$$

and using (3), (4), (8) and (9) we can explicitly write  $\rho(s)$  as ( $pp$  and  $\bar{p}p$ )

$$\rho^{pp}(s) = \frac{\frac{k}{s} + \frac{\pi}{2} \left[ -\frac{\delta(6+\gamma)}{s^{6+\gamma}} + \frac{\pi\beta\sqrt{2}}{m_\pi^2 s^\alpha} \left( \ln s - \frac{\alpha \ln^2 s}{2} \right) \right] + \frac{\pi}{4} [\sigma_{\text{tot}}^{pp} - \sigma_{\text{tot}}^{\bar{p}p}]}{\frac{\delta}{s^{6+\gamma}} + \frac{\pi\beta}{\sqrt{2}m_\pi^2 s^\alpha} \ln^2 s}, \quad (10)$$

$$\rho^{\bar{p}p}(s) = \frac{\frac{k}{s} + \frac{\pi}{2} \left[ -\frac{\bar{\delta}(6+\bar{\gamma})}{s^{6+\bar{\gamma}}} + \frac{\pi\bar{\beta}\sqrt{2}}{m_\pi^2 s^{\bar{\alpha}}} \left( \ln s - \frac{\bar{\alpha} \ln^2 s}{2} \right) \right] - \frac{\pi}{4} [\sigma_{\text{tot}}^{pp} - \sigma_{\text{tot}}^{\bar{p}p}]}{\frac{\bar{\delta}}{s^{6+\bar{\gamma}}} + \frac{\pi\bar{\beta}}{\sqrt{2}m_\pi^2 s^{\bar{\alpha}}} \ln^2 s}. \quad (11)$$

The only free parameter in the above results is the subtraction constant  $k$ . It is not difficult to see that  $\rho(s) = \rho \rightarrow \ln^{-1} s$  as  $s \rightarrow \infty$ . In the next sections, we shall show both individual and simultaneous fit results to  $\sigma_{\text{tot}}$  and  $\rho$  parameter.

#### IV. INDIVIDUAL FIT RESULTS FOR $\sigma_{\text{tot}}$ AND $\rho$

Available experimental data on  $\sigma_{\text{tot}}$  for proton-proton and antiproton-proton scattering were fitted by functions (3) and (4) respectively. The database compiled by Particle Data Group has become a standard references and the corresponding computer readable files are used [34]. The statistic and systematic errors are added linearly in our analysis just as well as for some early analysis (see, for example [35–37]).

As seen the suggested parameterizations are valid only for  $s \geq s_{\min}$ , where  $s_{\min}$  is some empirical low boundary (in GeV). During the analysis procedure we decrease the  $s_{\min}$  value as much as possible in order to describe the wider energy domain with statistically reasonable fit quality. This logic is used in all our fit procedure below. Thus the fits have been made only at  $s \geq s_{\min}$  for different values of low boundary. The fitting parameter values are presented in Table I for  $pp$  and in Table II for  $\bar{p}p$ . Figure 1 shows the experimental energy dependence for fit for  $pp$  (Fig. 1a),  $\bar{p}p$  (Fig. 1b) and corresponding fits at  $\sqrt{s_{\min}} = 5$  (red lines),  $\sqrt{s_{\min}} = 30$  (blue lines).

Parametrization (3) agree to experimental data very well for any  $\sqrt{s_{\min}}$  under study. One needs to emphasize that (3) allows us to describe experimental points at  $\sqrt{s_{\min}} = 3$  very well. We do not see clear energy dependence of  $\alpha$  and  $\beta$  within error bars but these parameters are very small and agree to expected values (Table I). One can see the statistically acceptable fit qualities are obtained for  $\sqrt{s_{\min}} = 5 - 15$  only for  $\bar{p}p$  (Table II). Fit function (4) agree to experimental points at qualitative level well for other low boundary values under study. But fit quality is statistically unacceptable at lowest  $\sqrt{s_{\min}}$  and some worse for  $\sqrt{s_{\min}} = 20 - 30$ <sup>1</sup>. The  $\bar{\alpha}$  as well as  $\bar{\beta}$  some decrease up to  $\sqrt{s_{\min}} = 10$  and remain almost constants within errors at larger  $\sqrt{s_{\min}}$ . On the other hand it seems small values of  $\alpha$ ,  $\bar{\alpha}$  agree with predicted behavior  $\sigma_{\text{tot}}^{NN} \propto \ln^2 s$  at high energies. One needs to emphasize the constraints (6) are valid for fits at  $\sqrt{s_{\min}} \geq 15$  within errors.

In accordance with (3) and (4) total cross-section energy dependence is described by the same functional form for  $pp$  and  $\bar{p}p$  reactions. Thus one can make the quantitative analysis of common data ensemble for  $\sigma_{\text{tot}}^{pp}$  and  $\sigma_{\text{tot}}^{\bar{p}p}$  taking into account above results. The fitting parameter values are presented in Table III for  $NN$  scattering. As seen the fit quality is statistically unacceptable for  $\sqrt{s_{\min}} = 15$  despite of equality of fit parameters for  $pp$  and  $\bar{p}p$ . Our quantitative analysis demonstrates that experimental data for  $pp$  and  $\bar{p}p$  total cross-section can be described by one function at  $\sqrt{s_{\min}} \geq 25$  with statistically reasonable quality. Fig. 2 shows the experimental energy dependence for  $\sigma_{\text{tot}}^{NN}$  and corresponding fits for two various  $\sqrt{s_{\min}}$ : fit at low energy limit for simultaneous study of proton-proton and antiproton-proton scattering  $\sqrt{s_{\min}} = 15$  is shown by red line, blue line corresponds to the fit with best quality at  $\sqrt{s_{\min}} = 25$ .

If we fix the set parameters we are capable to obtain theoretical predictions for  $\sigma_{\text{tot}}$  at the RHIC, LHC and at the future HC energies. There are several predictions for the total cross-section covering a wide range, from 80 mb up to 230 mb and at Tevatron ( $\sqrt{s} = 1.8$  TeV)  $\sigma_{\text{tot}}$  is ill-determined,  $\sigma_{\text{tot}} = (71.42 \pm 2.41)$  mb for E710 Collaboration and  $\sigma_{\text{tot}} = (80.03 \pm 2.24)$  mb according to CDF Collaboration. Using  $\sqrt{s_{\min}} = 5$  as the minimum low boundary value with statistically acceptable fit quality for  $\bar{p}p$  data one obtains  $\sigma_{\text{tot}}^{\bar{p}p} = (73.22 \pm 8.30)$  mb as a prediction for  $\sqrt{s} = 1.8$  TeV.

On the other hand, for  $\sqrt{s} = 546$  GeV (closest to the maximum RHIC energy), CDF Collaboration obtains  $\sigma_{\text{tot}} = (61.3 \pm 1.0)$  mb, UA4 Collaboration  $\sigma_{\text{tot}} = (61.9 \pm 1.5)$  mb. Using  $\sqrt{s_{\min}} = 5$  one obtains  $\sigma_{\text{tot}}^{\bar{p}p} = (61.93 \pm 6.17)$  mb for  $\sqrt{s} = 546$  GeV.

At  $\sqrt{s} = 14$  TeV, Block *et al* predict  $\sigma_{\text{tot}}^{pp} = (108.0 \pm 3.4)$  mb [38] and Bourrely, Soffer and Wu predict  $\sigma_{\text{tot}}^{pp} = 103.5$  mb [39]. In Table IV our predictions are shown for the  $pp$  total cross-section at LHC energy ranges, the future HC and at RHIC. To summarize, our predictions indicate  $\sigma_{\text{tot}} \simeq 100.44$  mb at  $\sqrt{s} = 14$  TeV,  $\sigma_{\text{tot}} \simeq 95.99$  mb at  $\sqrt{s} = 10$  TeV, and  $\sigma_{\text{tot}} \simeq 91.35$  mb at  $\sqrt{s} = 7$  TeV (possible LHC new energies).

The extraction of the  $pp$  total cross-section from cosmic-ray experiments is based on the determination of proton-air production cross-section. The procedure is model-dependent [40]. The Fly's Eye Collaboration [41] using the Geometrical Scaling model obtain to  $pp$  at  $\sqrt{s} = 30$  TeV  $\sigma_{\text{tot}} = (122 \pm 11)$  mb. At same energy one obtains  $\sigma_{\text{tot}} = (110.69 \pm 19.32)$  mb at  $\sqrt{s_{\min}} = 3$  as well as lowest energy boundary with statistically acceptable fit quality for  $pp$  scattering. On the other hand, Gaisser, Sukhatme and Yodh [42] using the Fly's Eye result and the Chou-Yang prescription for the slope [43] obtained at  $\sqrt{s} = 40$  TeV for  $pp$  interaction  $\sigma_{\text{tot}} = 175_{-27}^{+40}$  mb. At same energy one obtains  $\sigma_{\text{tot}} = (114.60 \pm 20.55)$  mb. Of course, results from cosmic-rays presents a theoretical bias as noted by Nikolaev [44]. When the Akeno's result at  $\sqrt{s} = 30$  TeV ( $\sim 92$  mb) was corrected the corresponding  $\sigma_{\text{tot}}$  increase (amazing) on  $\sim 30$  mb.

Even at higher energies than that accessible in the present collider experiments, Baltrusaitis *et al* predicts  $\sigma_{\text{tot}}^{pp} = (120 \pm 15)$  mb at  $\sqrt{s} = 30$  TeV [41]. At same energy our prediction using the parameters obtained starting at  $\sqrt{s_{\min}} = 3$  is  $\sigma_{\text{tot}}^{pp} = (110.69 \pm 19.32)$  mb. Finally, Block and Cahn [45] obtain at very high energies ( $\sqrt{s} = 500$  TeV)  $\sigma_{\text{tot}}^{pp} = (316.00 \pm 5.46)$  mb and our prediction to the same energy is  $\sigma_{\text{tot}}^{pp} = (149.25 \pm 32.85)$  mb, almost half. It is important to stress that the fit qualities for (3) and (4) are better for standard PDG parametrization at  $\sqrt{s} \geq 5$  GeV and suggested parameterizations allows to represent nucleon-nucleon  $\sigma_{\text{tot}}$  energy dependencies in wide energy domain.

---

<sup>1</sup> Values of fit parameters are equals at  $\sqrt{s_{\min}} = 25$  and for  $\sqrt{s_{\min}} = 30$  because of absence of experimental  $\bar{p}p$  points in the range of collision energies  $\sqrt{s} = 25 - 30$  GeV.

The experimental data for ratio of the real to imaginary part of the forward scattering amplitude are some poorer than that for total cross-sections especially in high energy domain. Below in this paragraph individual fits under study only for  $\rho$  parameter energy dependence in  $pp$  and  $\bar{p}p$  scattering.

The fitting functions (10) and (11) are used for  $\rho^{pp}(s)$  and for  $\rho^{\bar{p}p}(s)$  respectively.

There are two possible approaches for individual fit of  $\rho$  parameter for each interaction under considered, namely, i) the only one free parameter  $k$  is used in fitting functions (10) and (11) for  $\rho^{pp}(s)$  and for  $\rho^{\bar{p}p}(s)$  but values of all remain parameters are fixed by the individual fits of total cross-sections at corresponding  $\sqrt{s_{\min}}$ ; and ii) all parameters in (10) and (11) are free, results of individual fits for  $\sigma_{\text{tot}}^{pp}$  and  $\sigma_{\text{tot}}^{\bar{p}p}$  are not taken into account at all. The fit qualities are reasonable for any  $\sqrt{s_{\min}}$  both for  $pp$  (Table V, part i) and  $\bar{p}p$  (Table VI, part i) if the corresponding parameter values are fixed based on the above results for total cross-sections and only  $k$  parameter is free. Moreover,  $\chi^2/\text{n.d.f.}$  are statistically acceptable at  $\sqrt{s_{\min}} > 5$  for  $pp$  and at some values of  $\sqrt{s_{\min}}$  for  $\bar{p}p$  in the framework of i) fit approach. On the other hand the precision of  $k$  parameter is some poor especially for  $\bar{p}p$  interaction. The fit with all free parameters was studied also. The results for fit approach ii) are shown in Table V (part ii) for  $pp$  scattering and in Table VI (part ii) for  $\bar{p}p$  reaction<sup>1</sup>. For approach ii) high energy boundaries for individual fits of  $\rho$  have to be decreased because of large number of free parameters and small data samples for high energy domain. In this case the fit qualities are statistically acceptable for all  $s_{\min}$  under study both for  $pp$  and  $\bar{p}p$  interactions.

As seen from Table V and from Table VI precision of fit parameters is some poorer than that for total cross-section fits for both approaches i) and ii). Fig. 3 shows the experimental energy dependence of  $\rho$  parameter for  $pp$  (Fig. 3a,b), for  $\bar{p}p$  (Fig. 3c,d) elastic scattering and corresponding fits at various values of low boundary. Fits at  $\sqrt{s_{\min}} = 5$  are shown by red lines at all figures, fits at low boundary  $\sqrt{s_{\min}} = 30$  are available for i) approach only and shown by blue lines at Fig. 3a,c. The same color lines correspond to the  $\sqrt{s_{\min}} = 20$  (15) for  $pp$  ( $\bar{p}p$ ) reaction for ii) approach at Fig. 3b,d. In the framework of i) approach fit curves show a noticeable increasing /decreasing of  $\rho$  parameter value for  $pp$  /  $\bar{p}p$  interactions respectively for  $\sqrt{s_{\min}} = 3 - 10$  at high energies. The changing of absolute value of  $\rho$  is weaker at increasing of  $\sqrt{s_{\min}}$  (Fig. 3a,c). At higher values of low boundary fit curves for  $pp$  demonstrate some maximum value in the  $\sqrt{s} \sim 100$  GeV region but curves for  $\bar{p}p$  elastic scattering show the much more flat behavior than that for  $pp$  reaction. Value of the maximum for  $pp$  reaction increases with increasing of low boundary for fitted energy domain at  $\sqrt{s_{\min}} = 15 - 25$ . As seen from Fig. 3b the situation with increasing of low boundary is opposite in the framework of ii) approach for  $pp$ . The fit curves at Fig. 3d show increasing of  $\rho$  parameter for  $\bar{p}p$  interaction at any  $\sqrt{s_{\min}}$  under considered for ii) approach. It seems the model curves obtained in the framework of i) approach with one  $k$  free parameter show more reasonable and expected behaviour in the physics sense at  $\sqrt{s_{\min}} \geq 15$  at least than that in the framework of ii) approach. One can see a very small values for  $\beta$  at two highest values of  $\sqrt{s_{\min}}$  and for  $\bar{\beta}$  parameters in the case of individual fits of  $\rho^{pp/\bar{p}p}$  energy dependence. In the framework of ii) approach constraints (6) are valid for all fit parameters with exception of  $(\delta, \bar{\delta})$  pair at highest  $\sqrt{s_{\min}} = 15$  at which comparison is available for parameter values for  $pp$  and  $\bar{p}p$  reactions. But one needs to emphasize that qualities for individual fits are well enough for  $\sqrt{s_{\min}} = 3$  even and suggested formulas (10), (11) allow us to get a good agreement between model curves and experimental data in wide energy domain  $\sqrt{s} \geq 3$  GeV.

## V. SIMULTANEOUS FIT RESULTS FOR $\sigma_{\text{tot}}$ AND $\rho$

The simultaneous fits were considered for various ensembles for scattering parameters. Results of simultaneous fit for  $\{\rho^{pp}, \rho^{\bar{p}p}\}$  by (10) and (11) with all free parameters are shown at Fig. 4a and Fig. 4b for  $pp$  and  $\bar{p}p$ , respectively. Significant increasing of fitted points allows us to study the approximation of  $\rho$ -parameter energy dependence up to highest  $\sqrt{s_{\min}} = 30$ . Numerical values of fit parameters are in the Table VII. As seen fit qualities are statistical acceptable at  $\sqrt{s_{\min}} \geq 3$ . Parameter errors are the same order or some smaller than that for individual fits at corresponding  $\sqrt{s_{\min}}$ . Constraints (6) are valid at  $\sqrt{s_{\min}} \geq 15$  for all parameters within two standard deviations at least. Approximation curves show smooth behavior at all  $\sqrt{s_{\min}}$ . Some decreasing of  $\rho^{pp}$  is observed at high energies (Fig. 4a). This changing of  $\rho^{pp}$  at high energies is most noticeable at  $\sqrt{s_{\min}} = 15$ . Approximation curves are very close for  $\rho^{\bar{p}p}$  for  $0.03 \geq \sqrt{s} \leq 1$  TeV at all  $\sqrt{s_{\min}}$  under considered. Behaviour of fit curves for  $\rho^{\bar{p}p}(s)$  depends on value of  $\sqrt{s_{\min}}$ . At  $\sqrt{s_{\min}} = 15$  and 30 corresponding curves demonstrate almost constant value  $\rho^{\bar{p}p} \sim 0.12$  in  $\sqrt{s} > 100$  GeV energy domain. But model curves show decreasing at high energies  $\sqrt{s} > 1$  TeV at all another values of low boundary.

<sup>1</sup> Values of fit parameters are equals at  $\sqrt{s_{\min}} = 5$  and for  $\sqrt{s_{\min}} = 10$  because of absence of experimental  $\bar{p}p$  points in the range of collision energies  $\sqrt{s} = 5 - 10$  GeV.

Simultaneous fits for  $\{\sigma_{\text{tot}}^{pp}, \sigma_{\text{tot}}^{\bar{p}p}, \rho^{pp}\}$  by (3), (4) and (10) are shown at Fig. 5 for  $\sqrt{s_{\text{min}}} = 5$  (red lines) and for  $\sqrt{s_{\text{min}}} = 30$  (blue line). The values of fit parameters are shown in Table VIII. Suggested parameterizations allow us to obtain statistically acceptable fit qualities at  $\sqrt{s_{\text{min}}} \geq 5$  but fit quality is quite reasonable even at lowest  $\sqrt{s_{\text{min}}} = 3$ . The precisions are reasonable for all parameters. Constraints (6) are valid at  $\sqrt{s_{\text{min}}} \geq 15$  for all parameters (with exception of  $\delta, \bar{\delta}$  at two lowest  $\sqrt{s_{\text{min}}} = 15, 20$  under considered in this case) within two standard deviations at least. Total cross-section curves for  $pp$  show a very close behavior both for  $\sqrt{s_{\text{min}}} = 5$  and  $\sqrt{s_{\text{min}}} = 30$ . Model curve for  $\sigma_{\text{tot}}^{\bar{p}p}$  at  $\sqrt{s_{\text{min}}} = 5$  shows significantly slow increasing for high energy domain than that at  $\sqrt{s_{\text{min}}} = 30$ . The approximation curve for  $\rho^{pp}$  at  $\sqrt{s_{\text{min}}} = 5$  demonstrates the opposite behaviour at collision energy increasing in high energy domain ( $\sqrt{s} > 1$  TeV) than that the curve at highest low boundary for fitted energy domain.

Results for simultaneous fits of  $\{\sigma_{\text{tot}}^{pp}, \sigma_{\text{tot}}^{\bar{p}p}, \rho^{\bar{p}p}\}$  by (3), (4) and (11) are shown at Fig. 6 and in Table IX. Conclusions based on the numerical parameter values are similar them which have described above for Table VIII. One can see that fit parameters have a close values both in Table VIII and in Table IX at the same value of lower boundary for energy domain at  $\sqrt{s_{\text{min}}} \geq 3$  with exception of  $k$ -parameter. The total cross-section for  $\bar{p}p$  shows significantly slow increasing in high energy domain at  $\sqrt{s_{\text{min}}} = 5$  than that at  $\sqrt{s_{\text{min}}} = 30$  for the ensemble of scattering parameters under study (Fig. 6b). Behaviour of model curves for  $\rho^{\bar{p}p}$  at high energies depends on value of low boundary. The curves show noticeable decreasing at  $\sqrt{s_{\text{min}}} = 5 - 15$  for energy range  $\sqrt{s} > 1$  TeV. But fit curves demonstrate almost constant value  $\rho^{\bar{p}p} \sim 0.10 - 0.15$  at higher values of low boundary for energy domain indicated above.

Simultaneous fits of full set of global scattering parameters  $\{\sigma_t^{pp}, \sigma_t^{\bar{p}p}, \rho^{pp}, \rho^{\bar{p}p}\}$  by (3), (4), (10) and (11) are shown at Fig. 7 at  $\sqrt{s_{\text{min}}} = 5$  (red lines) and at  $\sqrt{s_{\text{min}}} = 30$  (blue lines). Numerical values of fit parameters are shown in Table X. Fit quality is statistically acceptable for  $\sqrt{s_{\text{min}}} \geq 5$ . Moreover fit quality is reasonable at lowest value of  $\sqrt{s_{\text{min}}}$  under study. Thus fit functions (3), (4), (10) and (11) allow us to obtain a reasonable description of experimental energy dependencies of global scattering parameters in wide energy domain. On the other hand one needs to emphasize that noticeable increasing (decreasing) of  $\rho^{pp}$  ( $\rho^{\bar{p}p}$ ) value is observed for high energies at  $\sqrt{s_{\text{min}}} \leq 10$  (Fig. 7c,d) especially at lowest boundary value  $\sqrt{s_{\text{min}}} = 3$ . At larger  $\sqrt{s_{\text{min}}}$  there is a maximum in  $\rho(s)$  dependence with following much slower decreasing of  $\rho$  for energy domain  $\sqrt{s} > 1$  TeV both in proton-proton and antiproton-proton interactions. Precisions are reasonable for all fit parameters at any low boundary values. These precisions are the same order or some smaller for this case than that for individual fits of scattering parameters. Constraints (6) are valid for all fit parameters at  $\sqrt{s_{\text{min}}} \geq 20$  within errors with exception for  $\delta$  and  $\bar{\delta}$ . The last two parameters have similar values, which are approached to each other with boundary value increasing. For  $\delta$  and  $\bar{\delta}$  parameters constraints (6) are valid at  $\sqrt{s_{\text{min}}}$  indicated above within two standard deviations. Parameters  $\alpha, \bar{\alpha}, \beta, \bar{\beta}$  are almost constants within errors for  $\sqrt{s_{\text{min}}} \geq 15$ .

The expected asymptotic behaviors are obtained for approximation curves for all scattering parameters under study at highest value of low boundary at least (Fig. 7). Curves for both  $pp$  and  $\bar{p}p$  cross-sections shows a close behavior at all  $\sqrt{s_{\text{min}}}$  especially for proton-proton interactions. Corresponding curves for  $\sigma^{\bar{p}p}$  demonstrate some differences for energies higher than 1 TeV at low  $\sqrt{s_{\text{min}}} \leq 5$  only. Difference between curves for  $\rho^{pp}$  ( $\rho^{\bar{p}p}$ ) at several  $\sqrt{s_{\text{min}}}$  are larger, especially for  $\sqrt{s} \geq 1$  TeV energy domain.

Predictions are obtained for  $\sigma_{\text{tot}}^{pp}, \sigma_{\text{tot}}^{\bar{p}p}$  at various energies based on the fit results of full set of global scattering parameters from Table X. Total cross-section values are shown in the Table XI. These results are in agreement with predictions above from Table IV. Uncertainties for these predictions are the same order or smaller for the case under considered than results, which were obtained for individual fits (Table IV). The smallest uncertainties are at  $\sqrt{s_{\text{min}}} = 15$ . Perhaps, the one of the reasons for such feature is the optimal value of low boundary  $\sqrt{s_{\text{min}}}$  which allows to exclude the influence of spread of experimental points at low energies on uncertainties of fit parameters as well as to remain amounts of experimental data large enough for reasonable precision of fit. As seen from the Table XI results for various  $\sqrt{s_{\text{min}}}$  are in a good agreement within errors.

Our results coincide well with values of  $\sigma_{\text{tot}}^{\bar{p}p}$  measured by UA4 and CDF Collaborations at  $\sqrt{s} = 546$  GeV at any  $\sqrt{s_{\text{min}}}$ , in particular, at  $\sqrt{s_{\text{min}}} = 15$  which correspond to the best precision for predictions as well as statistically acceptable fit quality (see Table X). The similar situation at higher energy  $\sqrt{s} = 1.8$  TeV taking into account the wider dispersion of experimental values obtained by E710 and CDF Collaborations. For  $\sqrt{s_{\text{min}}}$  under considered above our predictions are in good agreement with Fly's Eye Collaboration [41] data at  $\sqrt{s} = 30$  TeV but results in Table XI are in qualitative agreement only with the estimation  $\sigma_{\text{tot}}^{pp}$  at  $\sqrt{s} = 40$  TeV [42] with taking into account errors. Total cross-section value at very high energy  $\sqrt{s} = 500$  TeV significantly smaller than that from [45] as well as corresponding value obtained for individual fit results.

It is important to stress that simultaneous fits are used because at high energies  $pp$  and  $\bar{p}p$  elastic scattering amplitudes are (practically) the same function. Then,  $pp$  and  $\bar{p}p$  experimental data tend to the same value at high energies and we expect that the absence of  $pp$  experimental data at some high energy value may be filled by presence of  $\bar{p}p$  experimental data at (almost) same energy and vice-versa. Therefore, we expect that  $pp$  and  $\bar{p}p$  simultaneous fit allows more reliable numerical results to the fit parameters. As can be viewed in Tables IV and X the errors in the parameters obtained from simultaneous fits are the same order or some smaller than those from individual fits



allowing a more precise description of the fitted physical quantity.

Based on the above study one can conclude that suggested approximations allow to obtain fits (both individual and simultaneous) of experimental data for global scattering parameters with good statistical qualities for wide energy domain  $\sqrt{s} \geq 5$  GeV. Moreover this energy domain can be expanded as  $\sqrt{s} \geq 3$  GeV in some cases. The quality of last simultaneous fit at  $\sqrt{s_{\min}} = 10$  is better than that for Kang-Niculescu model fit as well as for Donnachie-Landshoff fit of  $pp$  and  $\bar{p}p$  experimental data [35]. Fit qualities obtained in this work for wide energy domains are close to the best fit qualities observed previously for various process in the framework of model with different number of poles [21, 22, 46, 47].

## VI. COMPARISONS

In this section, we compare the possible physical description of our model with some models present in the literature. There are several models but for the sake of the simplicity, we restrict ourselves to three models only. The first one is the famous and successful Donnachie-Landshoff model [48] based on a very simple parametrization structure evolving the exchange of reggeons and pomerons trajectories. The second one is the Kharzeev-Levin model [49–51] based on N=4 Super-symmetric Yang-Mills theory and considering the contribution of D-instantons for multiparticle production. Finally, the Godbole-Grau-Pancheri-Srivastava model [52–54] based on minijet contributions to the total cross-section.

### A. Donnachie-Landshoff Model

One of the most successful models is the Donnachie-Landshoff (DL) parametrization [48]

$$\sigma_{\text{tot}}^{pp}(s) = X s^\epsilon + Y^{pp} s^{-\eta}, \quad \sigma_{\text{tot}}^{\bar{p}p}(s) = X s^\epsilon + Y^{\bar{p}p} s^{-\eta}, \quad (12)$$

where  $X$ ,  $Y^{pp}$ ,  $Y^{\bar{p}p}$ ,  $\epsilon$ , and  $\eta$  are fit parameters. The first term on the right hand side of the above expressions ( $X = 21.7$  and  $\epsilon \approx 0.08$ ) is associated with the pomeron contribution and has a common value to both  $pp$  and  $\bar{p}p$  cross-section because the pomeron carries the quantum number of the vacuum and cannot distinguish particles and antiparticles. The second term ( $Y^{pp} \approx 56.1$ ,  $Y^{\bar{p}p} \approx 98.4$  and  $\eta \approx 0.45$ ) is associated with the reggeon trajectory, and it may be different to particles and antiparticles at low  $s$ . This term may be identified as resulting from  $\rho$ ,  $\omega$ ,  $f_2$ ,  $a_2$  exchange, for example. At  $s \rightarrow \infty$ , the difference between  $pp$  and  $\bar{p}p$  total cross-section parametrization can increase at most as  $\ln s$ . However, the difference may vanish if  $\sigma_{\text{tot}}^{pp} = \sigma_{\text{tot}}^{\bar{p}p}$  and, in any case, the ratio between both total cross sections tends to 1 as stated by the Pomeranchuk theorem.

The DL model possesses clearly two regimes. Roughly speaking, at low energy the second term at the right hand side of Eqs. (12) is the leading one (the reggeon exchange dominates) and at high energy regime, the first term will be the leading one (the pomeron exchange dominates). This picture is quite similar to our model where the first term of the right hand side of (3) and (4) is the sub-leading one and may be associated to the exchange of a reggeon trajectory with intercept  $\alpha_R(0) \approx 0.95$ .

On the other hand, using (5) we may connect (at high energies) the behavior of the leading term of our model with the exchange of a pomeron trajectory. Adopting  $c = 21.7$  as obtained in the DL model we obtain  $p \leq 0.06$  and therefore,  $\alpha_P(0) \leq 1.06$ . This value is slightly above 1 and may lead to the violation of the Froissart-Martin bound, but it does not occur for momenta lower than Planck scale. In this way, the pomeron exchange mechanism may ensure the preservation of unitarity.

However, comparisons done above are not exactly correct. In our model, at low energies, reggeon and pomeron trajectories interact with each other mixing the intercept contributions. Therefore, the reggeon intercepts showed here present pomeron contributions. Indeed,  $f_2$  trajectory, for example, has the quantum number of the vacuum as the pomeron. There may be contributions from pomerons at low energies, preventing the complete separation between pomerons and reggeons. We expect, at high energies, the divergence of reggeon and pomeron trajectories from each other. Then, the influence of reggeons will cease and only the pomeron exchange will be the main physical mechanism restoring the validity of Pomeranchuk theorem.

### B. Kharzeev-Levin Model

The Kharzeev-Levin (KL) model [49–51] is based on the Super-symmetric Yang-Mills theory in N=4 (N=4 SYM). Considering contributions of D-instantons in  $AdS_5$  bulk space, they argue that D-instantons coupled to dilatons and

axions are responsible for multiparticle production in strongly coupled N=4 SYM. As a consequence, the cross-section increases with the energy

$$\sigma_{\text{inel}} \propto s^{\Delta-2},$$

where  $\Delta$  depends on the convenient choice of parameters [49–51]. This approach is interesting since it suggests that topological effects may be important in high energy collisions. Furthermore, they argue that the weakly coupled graviton generates the elastic amplitude and the correspondent part of the total cross-section. On the other hand, D-instanton induced interactions of dilatons and axions are responsible for the multiparticle production processes.

This formalism predicts that the cross-section will increase with the energy due to D-instanton mechanism. This mechanism is induced by interactions of dilatons and axions responsible for the multiparticle production process. The pomeron intercepts predicted in KL model depends on the value of  $\Delta$  (and  $\sigma_{\text{inel}} \propto s^{\Delta-2}$ ). They found  $\Delta \approx 4$  and consequently, the slope  $\alpha'_p \approx 0.5 \text{ GeV}^{-2}$ .

However, this value of  $\Delta$  may imply in a strong unitarisation scheme to restore the Froissart-Martin bound. As shown above, the pomeron exchange may be the main mechanism responsible for restore the unitarisation. Indeed, they obtain a very high pomeron intercept, possibly indicating the exchange of a new soft pomeron trajectory family ( $\Delta$  is not unique).

The model proposed here possesses a very smooth increase (at high energies) when compared with the standard theoretical result  $\sigma_{\text{tot}} \approx 60 \ln^2 s$ . The KL model may explains these differences in the behaviors by the mechanism of multiparticle production: at high energies the multiparticle mechanism acts, increasing the hadron cross-section and when the saturation limit approaches the pomeron exchange has become physically important restoring the unitarity scheme turning the increase of the total cross-section smooth as obtained. Moreover, we may suppose a mixed state "reggeon+pomeron" as being the responsible for the observed differences between  $pp$  and  $\bar{p}p$  total cross-section.

### C. Godbole-Grau-Pancheri-Srivastava Model

The study of QCD minijet contribution is the main goal of the Godbole-Grau-Pancheri-Srivastava (GGPS) model [52–54]. This model includes a re-summation of soft gluon radiation which they argue it is necessary to tame the fast high energy rise typical of a purely perturbative minijet model.

The minijet formalism predicts a very fast rise to  $\sigma_{\text{jet}} \approx s^{0.3}$  at high energies. To restore the total cross-section they suppose that soft gluon emissions from the colliding partons are the physical attenuation mechanism. To restore the Froissart-Martin bound, they obtain a "new" formulation of the Froissart-Martin bound

$$\sigma_{\text{tot}} \sim (\epsilon \ln s)^{1/n}$$

where  $\epsilon$  fixes the asymptotic rise and  $1/2 < n < 1$  modulates the infrared behavior of  $\alpha_s$  [52–54].

Pomeron exchange is believed to be the exchange of a system of gluons. Therefore (ultimately), the pomeron exchange will be the Froissart-Martin bound restoration mechanism as in the KL model. As seen above, the pomeron exchange has a very important role if we want to understand the taming mechanism behind no saturation effect in our model.

## VII. FINAL REMARKS

The model proposed here to describe the hadron-hadron total cross-section and the  $\rho$  parameter is basically based on two rigorously bounds obtained in the framework of AQFT. Namely, the Froissart-Martin bound and Jin-Martin-Cornille bound. Roughly speaking, in this model the like-Froissart-Martin bound will control the high energy behavior of the total cross-section, and like-Jin-Martin-Cornille bound will defines its behavior at low energies. However, the analysis of our model is not so simple, since we suppose an attenuation mechanism in the Froissart-Martin bound  $\sim s^{-\alpha} \ln^2 s$  which mix these two bounds, especially at low energies.

The statistical description of  $\sigma_{\text{tot}}$  and  $\rho$  experimental data is acceptable. The quality of some simultaneous fits is better than that for Kang-Nicolescu model fit as well as for Donnachie-Landshoff fit of  $pp$  and  $\bar{p}p$  experimental data. The qualities of the fits obtained in this work for wide energy domains are closer to the best fit qualities previously observed for several processes in the framework of the model with a different number of poles. Therefore, based on this statistical fact, it is possible perform predictions in the energy variable and the results can be compared with others present in some models and parameterizations in available literature. Results viewed here shown some agreement among themselves.

Comparisons with some models may allow some physical understanding of what is happening here. In the context of DL model, we may understand the the index in the low energy term of our model as representing a reggeon exchange trajectory, and the index in the high energy term - as a pomeron exchange trajectory. Yet, the picture viewed here seems to be not so simple. The mixed description proposed, especially at low energies, prevents the identification of each index contribution separately (or each trajectory separately) and, therefore, we cannot treat this low energy term as being a pure reggeon exchange.

In the context of KL and GGPS models, the pomeron exchange is the responsible for the attenuation of the rise of the total cross-section. However, in both models the saturation of the total cross-section is quickly reached and therefore, it is necessary the exchange of not only one pomeron but a whole family. In our model, this attenuation mechanism may be explained by the interaction of pomerons and reggeons that tames the rise of the total cross-section and this mixed state of index (trajectories) may be responsible for the observed differences between  $pp$  and  $\bar{p}p$  behaviors.

On the other hand, the model presented here does not saturate the total cross-section. Then, we may suppose that this is due to the exchange of more than only one pomeron trajectory since the increase of experimental data set in the fit procedures may give rise to different values of the effective index  $p$  and each value may represent a novel pomeron trajectory. Therefore, novel experimental results to total cross section can be added to the original data set allowing more precise values to the effective index  $p$  through fit procedures. These trajectories may tend to a limiting value, i.e,  $p_i \rightarrow p_l$  where  $i$  represents a pomeron trajectory and  $l$  represents the limiting trajectory ( $\alpha_{P_i}(0) \rightarrow \alpha_{P_l}(0)$ ). If this pomeron trajectory limit exist it may represent a definite (or not, since a new physical attenuation mechanism may be discovered) bound to the rise of total cross section. This behavior at very high energies is one of the puzzles to be solved at the future HC because the applied mechanisms used to tame its very fast rise, we hope, will be verified.

### Acknowledgments

S.D.C is grateful to UFSCar for the financial support. The work of V.A.O. was supported partly by the Russian Federal Agency for Science and Innovation grant (State Contract No. 02.740.11.2040).

- 
- [1] P.V. Landshoff and O. Nachtmann, *Z. Phys. C* **35**, 405 (1987).
  - [2] Y. Afek, C. Leroy, B. Margolis and P. Valin, *Phys. Rev. Lett.* **45**, 85 (1980).
  - [3] L. Durand and H. Pi, *Phys. Rev. Lett.* **58**, 303 (1987).
  - [4] L. Durand and H. Pi, *Phys. Rev. D* **38**, 78 (1988).
  - [5] L. Durand and H. Pi, *Phys. Rev. D* **40**, 1436 (1989).
  - [6] M.M. Block, E.M. Gregores, F. Halzen and G. Pancheri, *Phys. Rev. D* **60**, 054024 (1999).
  - [7] J.M. Cornwall, *Phys. Rev. D* **26**, 1453 (1982).
  - [8] J.M. Cornwall and J. Papavassiliou, *Phys. Rev. D* **40**, 3474 (1989).
  - [9] J. Papavassiliou and J.M. Cornwall, *Phys. Rev. D* **44**, 1285 (1991).
  - [10] M.B. Gay Ducati, F. Halzen and A.A. Natale, *Phys. Rev. D* **48**, 2324 (1993).
  - [11] F. Halzen, G. Krein and A.A. Natale, *Phys. Rev. D* **47**, 295 (1993).
  - [12] A.C. Aguilar, A. Mihara and A.A. Natale, *Phys. Rev. D* **65**, 054011 (2002).
  - [13] A.C. Aguilar, A. Mihara and A.A. Natale, *Int. J. Mod. Phys. A* **19**, 249 (2004).
  - [14] A.C. Aguilar, P.S.R. da Silva and A.A. Natale, *Phys. Rev. Lett.* **90**, 152001 (2003).
  - [15] R.F. Ávila, S.D. Campos, M.J. Menon and M. Montanha, *Eur. Phys. J. C* **47**, 171 (2006).
  - [16] M. Froissart, *Phys. Rev.* **123**, 1053 (1961).
  - [17] A. Martin, *Il Nuovo Cimento A* **42**, 930 (1966).
  - [18] Y.S. Jin and A. Martin, *Phys. Rev.* **135**, B1369 (1964).
  - [19] H. Cornille, *Nuovo Cimento A* **4**, 549 (1971).
  - [20] M.M. Block, K. Kang and A.R. White, *Int. J. Mod. Phys. A* **7**, 4449 (1992).
  - [21] J.R. Cudell, V. Ezhela, P. Gauron, K. Kang, Yu.V. Kuyanov, S. Lugovsky, B. Nicolescu and N. Tkachenko, *Phys. Rev. D* **65**, 074024 (2002).
  - [22] COMPETE Collab. (J.R. Cudell *et al.*), *Phys. Rev. Lett.* **89**, 201801 (2002).
  - [23] G. Matthiae, *Rep. Prog. Phys.* **57**, 743 (1994).
  - [24] R.J. Eden, *Rev. Mod. Phys.* **43**, 15 (1971).
  - [25] G. Grumberg and T.N. Truong, *Phys. Rev. Lett.* **31**, 63 (1973).
  - [26] J.D. Jackson, Phenomenology of Particles at High Energies, in *Proc. of the Fourteenth Scottish Universities Summer School in Physics*, eds. R.L. Crawford and R. Jennings (Academic Press 1974), p. 1.
  - [27] R.F. Ávila and M.J. Menon, *Nucl. Phys.* **A744**, 249 (2004).

- [28] J.B. Bronzan, G.L. Kane and U.P. Sukhatme, *Phys. Lett.* **B49**, 272 (1974).
- [29] K. Kang and B. Nicolescu, *Phys. Rev.* **D11**, 2461 (1975).
- [30] S. Goldberg, *Unbounded Linear Operators*, McGraw-Hill Inc. (1966).
- [31] J. Fischer and P. Kolář, *J. Math. Phys.* **25**, 2538 (1984).
- [32] J. Fischer and P. Kolář, *Phys. Lett. B* **64**, 45 (1976).
- [33] J. Fischer and P. Kolář, *Phys. Rev.* **D17**, 2168 (1978).
- [34] Particle Data Group (W.-M. Yao, C. Amsler, D. Asner *et al.*), *J. Phys. G* **33**, 1 (2006).
- [35] R.F. Ávila, E.G.S. Luna and M.J. Menon, *Phys. Rev. D* **67**, 054020 (2003).
- [36] S.B. Nurushev and V.A. Okorokov, hep-ph/0711.2231 (2007).
- [37] S.B. Nurushev and V.A. Okorokov, Elastic Proton-Proton and Proton-Antiproton Scattering: Analysis of Complete Set of Helicity Amplitudes, *Proc. of the XII Advanced Research Workshop on High Energy Spin Physics*, eds. A.V. Efremov and S.V. Goloskokov, (JINR, Dubna 2007), p. 117.
- [38] M.M. Block, E.M. Gregores, F. Halzen and G. Pancheri, *Phys. Rev. D* **58**, 017503 (1998).
- [39] C. Bourrely, J. Soffer and T.T. Wu, *Eur. Phys. J. C* **28**, 97 (2003).
- [40] T.K. Gaisser, *Nucl. Phys. Proc. Suppl.* **12**, 172 (1990).
- [41] R.M. Baltrusaitis, G.L. Cassiday, J.W. Elbert, P.R. Gerhardy, S. Ko, E.C. Loh, Y. Mizumoto, P. Sokolsky and D. Steck, *Phys. Rev. Lett.* **52**, 1380 (1984).
- [42] T.K. Gaisser, U.P. Sukhatme and G.B. Yodh, *Phys. Rev. D* **36**, 1350 (1987).
- [43] T. Chou and C.N. Yang, *Phys. Lett. B* **128**, 457 (1983).
- [44] N.N. Nikolaev, *Phys. Rev. D* **48**, R1904 (1993).
- [45] M.M. Block and R.N. Cahn, *Rev. Mod. Phys.* **57**, 563 (1985).
- [46] J.R. Cudell, V. Ezhela and K. Kang, S. Lugovsky and N. Tkachenko, *Phys. Rev. D* **61**, 034019 (2000).
- [47] J.R. Cudell, A. Lenhyel and E. Martynov, *Phys. Rev. D* **73**, 034008 (2006).
- [48] A. Donnachie and P.V. Landshoff, *Phys. Lett. B* **296**, 227 (1992).
- [49] D.E. Kharzeev and E.M. Levin, hep-ph/9912216 (1999).
- [50] D.E. Kharzeev and E.M. Levin, hep-ph/0910.3355 (2009).
- [51] D.E. Kharzeev, Yu.V. Kovchegov and E.M. Levin, *Nucl. Phys. A* **690**, 621 (2001).
- [52] A. Achilli, R. Hedge, R.M. Godbole, A. Grau, G. Pancheri and Y. Srivastava, *Phys. Lett. B* **659**, 137 (2008).
- [53] R.M. Godbole, A. Grau, G. Pancheri and Y.N. Srivastava, *Phys. Rev. D* **72**, 076001 (2005).
- [54] A. Grau, G. Pancheri and Y.N. Srivastava, *Phys. Rev. D* **60**, 114020 (1999).

$\sqrt{s_{\min}}$	$\alpha$	$\beta \times 10^3$	$-\gamma$	$\delta$	$\chi^2/\text{n.d.f}$
3	0.028±0.008	3.9±0.3	5.882±0.005	51.8±0.5	107.6/139
5	0.020±0.010	3.4±0.5	5.890±0.010	50.8±1.5	74.9/107
10	0.010±0.012	2.9±0.6	5.910±0.020	48.5±2.8	46.7/69
15	0.010±0.008	2.9±0.3	5.906±0.005	48.8±1.0	34.2/58
20	0.019±0.003	3.6±0.1	5.876±0.004	54.8±1.1	30.1/45
25	0.031±0.002	4.6±0.1	5.821±0.009	69.5±4.2	15.9/33
30	0.021±0.012	3.7±0.9	5.870±0.040	55.7±10.1	15.1/30

TABLE I: Parameters for fitting by (3) of  $\sigma_{\text{tot}}^{pp}$  energy dependence.

$\sqrt{s_{\min}}$	$\bar{\alpha}$	$\bar{\beta} \times 10^3$	$-\bar{\gamma}$	$\bar{\delta}$	$\chi^2/\text{n.d.f}$
3	0.085±0.008	9.7±0.3	5.664±0.006	130.9±1.8	160.6/69
5	0.059±0.006	6.9±0.5	5.749±0.013	99.8±3.8	35.7/55
10	0.040±0.013	5.0±1.0	5.808±0.034	80.8±9.0	22.4/25
15	0.005±0.026	2.7±1.2	5.895±0.043	58.1±8.5	16.3/20
20	0.013±0.032	3.1±1.8	5.875±0.067	63.6±14.8	15.2/13
25	0.023±0.031	3.8±2.1	5.836±0.094	77.1±28.1	14.8/11

TABLE II: Parameters for fitting by (4) of  $\sigma_{\text{tot}}^{\bar{p}p}$  energy dependence.

$\sqrt{s}(\text{TeV})$	3	5	10	$\sqrt{s_{\min}}$ 15	20	25	30
	$\sigma_{\text{tot}}^{pp}$ (mb)						
0.2	51.95 ±4.32	51.06±6.62	52.09±9.09	51.42 ±4.58	52.42±1.73	52.84±1.74	52.0±12.3
0.5	60.46 ±6.14	59.66±9.15	61.0±12.2	60.29 ±6.55	61.82±2.41	62.64±2.06	61.3±15.5
7	91.4 ±13.7	92.6 ±19.7	96.7 ±26.0	96.1 ±15.3	98.04±5.53	97.92 ±3.98	96.8 ±29.7
10	96.0 ±15.0	97.7 ±21.5	102.6±28.5	102.0±16.8	103.75±6.09	103.13±4.33	102.3±32.2
14	100.4±16.3	102.7±23.3	108.3±30.9	107.7±18.4	109.26±6.64	108.09±4.67	107.7±34.6
30	110.7±19.3	114.4±27.7	122.0±37.0	121.4±22.3	122.20±8.01	119.42±5.50	120.2±40.5
40	114.6±20.6	118.9±29.4	127.4±39.5	126.8±23.9	127.23±8.56	123.71±5.83	125.0±42.9
50	117.7±21.5	122.4±30.8	131.6±41.5	131.1±25.2	131.18±9.00	127.04±6.09	128.8±44.7
100	127.2±24.7	133.7±35.5	145.4±48.2	144.9±29.4	143.7±10.5	137.35±6.94	140.7±50.9
200	136.7±28.1	145.3±40.4	159.8±55.4	159.3±34.1	156.5±12.1	147.56±7.84	152.9±57.4
500	149.3±32.9	160.8±47.5	179.8±66.1	179.4±41.0	173.9±14.3	160.79±9.10	169.3±66.7
	$\sigma_{\text{tot}}^{\bar{p}p}$ (mb)						
0.546	62.10±2.94	61.93±6.17	61.9±14.0	61.4±26.8	60.8±35.6	61.3±36.9	-
1.8	70.37±3.80	73.22±8.30	74.9±19.8	76.2±38.8	75.1±50.3	75.6±50.7	-

TABLE III: Predictions for  $\sigma_{\text{tot}}$  at various energies based on the individual fits of energy dependence of proton-proton and proton-antiproton total cross-sections.

$\sqrt{s_{\min}}$	$\alpha_{NN}$	$\beta_{NN} \times 10^3$	$-\gamma_{NN}$	$\delta_{NN}$	$\chi^2/\text{n.d.f}$
15	0.042±0.008	5.3±0.7	5.804±0.028	73.7±7.7	519.3/82
20	0.034±0.011	4.6±0.9	5.837±0.036	64.1±8.8	196.9/62
25	0.011±0.017	2.9±1.0	5.912±0.040	47.3±7.0	91.1/48
30	0.010±0.003	2.8±0.1	5.915±0.004	46.6±1.1	90.8/45

TABLE IV: Parameters for fitting by (3) of  $\sigma_{\text{tot}}^{NN}$  energy dependence.

Parameter	$\sqrt{s_{\min}}$						
	3	5	10	15	20	25	30
	i)						
$k$ , mbarn	$39 \pm 6$	$-0.5 \pm 17$	$-239 \pm 36$	$15 \pm 60$	$-115 \pm 104$	$571 \pm 239$	$648 \pm 301$
$\chi^2/\text{n.d.f.}$	146/80	93.9/63	39.1/47	32.3/33	13.8/22	1.53/9	0.16/6
	ii)						
$k$ , mbarn	$32 \pm 8$	$150 \pm 19$	$514 \pm 2$	$1202 \pm 2$	$40.0 \pm 1.4$	-	-
$\alpha$	$0.54 \pm 0.05$	$0.55 \pm 0.09$	$0.53 \pm 0.06$	$-0.20 \pm 0.11$	$-0.15 \pm 0.12$	-	-
$\beta \times 10^3$	$4.4 \pm 0.5$	$6 \pm 5$	$0.8 \pm 0.2$	$0.006 \pm 0.003$	$0.0011 \pm 0.0002$	-	-
$-\gamma$	$5.31 \pm 0.05$	$5.21 \pm 0.10$	$5.21 \pm 0.06$	$4.4 \pm 0.1$	$4.10 \pm 0.18$	-	-
$\delta$ , mbarn	$40 \pm 20$	$53 \pm 62$	$50 \pm 27$	$141 \pm 55$	$129 \pm 12$	-	-
$\bar{\alpha}$	$0.59 \pm 0.17$	$0.7 \pm 0.3$	$0.7 \pm 0.5$	$-0.18 \pm 0.07$	$-0.13 \pm 0.11$	-	-
$\bar{\beta} \times 10^3$	$0.66 \pm 0.07$	$2 \pm 2$	$0.057 \pm 0.005$	$0.01 \pm 0.01$	$0.0022 \pm 0.0003$	-	-
$-\bar{\gamma}$	$5.12 \pm 0.08$	$5.04 \pm 0.07$	$4.963 \pm 0.003$	$5.010 \pm 0.006$	$5.041 \pm 0.013$	-	-
$\bar{\delta}$ , mbarn	$51 \pm 3$	$181 \pm 38$	$733 \pm 6$	$1443 \pm 22$	$40 \pm 3$	-	-
$\chi^2/\text{n.d.f.}$	75.3/72	63.9/55	38.9/39	26.0/25	12.4/14	-	-

TABLE V: Parameters for individual fitting by (10) of  $\rho^{pp}$  energy dependence. Part i) corresponds to approach with one free parameter  $k$  and part ii) shows results for approach with all free parameters in (10).

Parameter	$\sqrt{s_{\min}}$						
	3	5	10	15	20	25	30
	i)						
$k$ , mbarn	$109 \pm 25$	$65 \pm 144$	$38 \pm 131$	$-436 \pm 172$	$-87 \pm 416$	$1172 \pm 1197$	$884 \pm 1197$
$\chi^2/\text{n.d.f.}$	44.4/17	20.8/11	16.6/11	2.73/10	8.21/6	11.7/4	7.60/4
	ii)						
$k$ , mbarn	$-0.3 \pm 0.2$	$15 \pm 3$	-	$18 \pm 3$	-	-	-
$\alpha$	$-0.4 \pm 0.2$	$0.078 \pm 0.016$	-	$-0.03 \pm 0.10$	-	-	-
$\beta \times 10^6$	$0.13 \pm 0.10$	$4.5 \pm 0.9$	-	$3 \pm 3$	-	-	-
$-\gamma$	$4.0 \pm 1.3$	$4.8 \pm 0.4$	-	$4.55 \pm 0.17$	-	-	-
$\delta$ , mbarn	$-5 \pm 4$	$10 \pm 11$	-	$61.5 \pm 48.2$	-	-	-
$\bar{\alpha}$	$-0.4 \pm 0.2$	$0.056 \pm 0.015$	-	$-0.05 \pm 0.10$	-	-	-
$\bar{\beta} \times 10^6$	$0.06 \pm 0.05$	$3.4 \pm 0.6$	-	$2.0 \pm 1.3$	-	-	-
$-\bar{\gamma}$	$5.52 \pm 0.02$	$5.07 \pm 0.06$	-	$5.12 \pm 0.12$	-	-	-
$\bar{\delta}$ , mbarn	$0.5 \pm 0.5$	$13 \pm 3$	-	$13 \pm 10$	-	-	-
$\chi^2/\text{n.d.f.}$	9.67/9	1.84/3	-	1.78/2	-	-	-

TABLE VI: Parameters for individual fitting by (11) of  $\rho^{\bar{p}p}$  energy dependence. Part i) corresponds to approach with one free parameter  $k$  and part ii) shows results for approach with all free parameters in (11).

Parameter	$\sqrt{s_{\min}}$						
	3	5	10	15	20	25	30
$k$ , mbarn	$11.7 \pm 3.5$	$21 \pm 7$	$-23 \pm 19$	$109 \pm 42$	$-242 \pm 68$	$-174 \pm 147$	$-200 \pm 189$
$\alpha$	$0.05 \pm 0.02$	$0.051 \pm 0.007$	$0.038 \pm 0.006$	$0.06 \pm 0.03$	$0.045 \pm 0.006$	$0.027 \pm 0.008$	$0.05 \pm 0.03$
$\beta \times 10^3$	$0.92 \pm 0.18$	$0.78 \pm 0.03$	$1.12 \pm 0.06$	$1.10 \pm 0.15$	$1.06 \pm 0.07$	$1.05 \pm 0.09$	$1.3 \pm 0.7$
$-\gamma$	$5.84 \pm 0.02$	$5.844 \pm 0.016$	$5.866 \pm 0.009$	$5.68 \pm 0.06$	$5.876 \pm 0.013$	$5.84 \pm 0.02$	$5.80 \pm 0.13$
$\delta$ , mbarn	$10.05 \pm 0.49$	$8.2 \pm 0.8$	$13.3 \pm 0.8$	$22 \pm 3$	$10.6 \pm 1.0$	$16 \pm 2$	$18 \pm 12$
$\bar{\alpha}$	$0.061 \pm 0.005$	$0.065 \pm 0.006$	$0.043 \pm 0.005$	$0.05 \pm 0.02$	$0.045 \pm 0.006$	$0.023 \pm 0.008$	$0.03 \pm 0.02$
$\bar{\beta} \times 10^3$	$1.18 \pm 0.10$	$1.05 \pm 0.05$	$1.28 \pm 0.08$	$0.91 \pm 0.09$	$1.11 \pm 0.09$	$0.94 \pm 0.11$	$0.9 \pm 0.3$
$-\bar{\gamma}$	$5.73 \pm 0.02$	$5.705 \pm 0.004$	$5.802 \pm 0.009$	$5.75 \pm 0.05$	$5.855 \pm 0.013$	$5.887 \pm 0.016$	$5.90 \pm 0.10$
$\bar{\delta}$ , mbarn	$19.7 \pm 2.5$	$18.7 \pm 0.6$	$20.6 \pm 1.1$	$16.2 \pm 1.9$	$12.2 \pm 1.1$	$12.9 \pm 1.5$	$11 \pm 6$
$\chi^2/\text{n.d.f.}$	86.6/90	66.3/67	42.1/51	29.8/36	12.8/21	1.18/6	0.25/3

TABLE VII: Parameters for simultaneous fitting by (10) and (11) of  $\rho$  energy dependencies for proton-proton and antiproton-proton collisions respectively.

Parameter	$\sqrt{s_{\min}}$						
	3	5	10	15	20	25	30
$k$ , mbarn	$42.0 \pm 6.5$	$-52 \pm 18$	$-131 \pm 42$	$32 \pm 20$	$107.6 \pm 74.5$	$671.4 \pm 426.5$	$621 \pm 454$
$\alpha$	$0.016 \pm 0.007$	$0.018 \pm 0.003$	$0.011 \pm 0.004$	$0.017 \pm 0.005$	$0.025 \pm 0.010$	$0.024 \pm 0.015$	$0.022 \pm 0.008$
$\beta \times 10^3$	$3.4 \pm 0.3$	$3.44 \pm 0.07$	$3.0 \pm 0.1$	$3.42 \pm 0.15$	$4.1 \pm 0.6$	$4.0 \pm 1.3$	$3.8 \pm 0.6$
$-\gamma$	$5.888 \pm 0.004$	$5.889 \pm 0.001$	$5.903 \pm 0.004$	$5.885 \pm 0.003$	$5.85 \pm 0.02$	$5.85 \pm 0.07$	$5.865 \pm 0.031$
$\delta$ , mbarn	$51.3 \pm 0.4$	$51.2 \pm 0.4$	$49.1 \pm 0.9$	$52.6 \pm 1.1$	$60 \pm 6$	$61 \pm 17$	$57 \pm 8$
$\bar{\alpha}$	$0.084 \pm 0.003$	$0.056 \pm 0.005$	$0.042 \pm 0.011$	$0.013 \pm 0.003$	$0.026 \pm 0.018$	$0.023 \pm 0.012$	$0.023 \pm 0.011$
$\bar{\beta} \times 10^3$	$9.6 \pm 0.3$	$6.4 \pm 0.5$	$5.15 \pm 0.90$	$3.13 \pm 0.13$	$4.0 \pm 1.3$	$4 \pm 2$	$4 \pm 2$
$-\bar{\gamma}$	$5.669 \pm 0.005$	$5.758 \pm 0.012$	$5.80 \pm 0.03$	$5.879 \pm 0.002$	$5.84 \pm 0.05$	$5.84 \pm 0.10$	$5.84 \pm 0.09$
$\bar{\delta}$ , mbarn	$129.3 \pm 1.7$	$97 \pm 3$	$83 \pm 9$	$61.8 \pm 1.2$	$74 \pm 14$	$77 \pm 34$	$77 \pm 31$
$\chi^2/\text{n.d.f.}$	392/288	182/225	109/141	81.1/111	60.2/80	31.7/53	30.1/47

TABLE VIII: Parameters for simultaneous fitting by (3), (4) and (10) of  $\sigma_{\text{tot}}^{pp}$ ,  $\sigma_{\text{tot}}^{\bar{p}p}$  and  $\rho^{pp}$  energy dependencies.

Parameter	$\sqrt{s_{\min}}$						
	3	5	10	15	20	25	30
$k$ , mbarn	$102 \pm 20$	$21 \pm 17$	$-91 \pm 39$	$-399 \pm 188$	$-585 \pm 208$	$-230 \pm 123$	$-270.5 \pm 109.7$
$\alpha$	$0.035 \pm 0.006$	$0.026 \pm 0.004$	$0.011 \pm 0.003$	$0.018 \pm 0.004$	$0.017 \pm 0.005$	$0.018 \pm 0.004$	$0.017 \pm 0.003$
$\beta \times 10^3$	$4.2 \pm 0.3$	$3.77 \pm 0.13$	$2.95 \pm 0.07$	$3.38 \pm 0.11$	$3.40 \pm 0.17$	$3.31 \pm 0.15$	$3.35 \pm 0.08$
$-\gamma$	$5.878 \pm 0.005$	$5.884 \pm 0.002$	$5.906 \pm 0.002$	$5.899 \pm 0.003$	$5.884 \pm 0.002$	$5.880 \pm 0.004$	$5.889 \pm 0.005$
$\delta$ , mbarn	$52.15 \pm 0.44$	$51.6 \pm 0.4$	$48.6 \pm 0.7$	$51.5 \pm 1.1$	$53.0 \pm 1.3$	$54.1 \pm 1.2$	$51.6 \pm 1.8$
$\bar{\alpha}$	$0.082 \pm 0.003$	$0.058 \pm 0.002$	$0.036 \pm 0.002$	$0.014 \pm 0.003$	$0.012 \pm 0.003$	$0.016 \pm 0.013$	$0.013 \pm 0.005$
$\bar{\beta} \times 10^3$	$9.4 \pm 0.3$	$6.63 \pm 0.12$	$4.69 \pm 0.13$	$3.15 \pm 0.11$	$3.09 \pm 0.11$	$3.3 \pm 0.7$	$3.2 \pm 0.2$
$-\bar{\gamma}$	$5.669 \pm 0.005$	$5.750 \pm 0.002$	$5.818 \pm 0.003$	$5.880 \pm 0.003$	$5.878 \pm 0.006$	$5.865 \pm 0.025$	$5.870 \pm 0.007$
$\bar{\delta}$ , mbarn	$129.7 \pm 1.7$	$99.6 \pm 0.8$	$78.1 \pm 1.3$	$61.3 \pm 1.4$	$63 \pm 3$	$67 \pm 7$	$65 \pm 5$
$\chi^2/\text{n.d.f.}$	288/225	115/173	72.3/105	53.4/88	46.6/64	31.7/48	30.9/45

TABLE IX: Parameters for simultaneous fitting by (3), (4) and (11) of  $\sigma_{\text{tot}}^{pp}$ ,  $\sigma_{\text{tot}}^{\bar{p}p}$  and  $\rho^{\bar{p}p}$  energy dependencies.

Parameter	$\sqrt{s_{\min}}$						
	3	5	10	15	20	25	30
$k$ , mbarn	$48 \pm 6$	$-51 \pm 18$	$-121 \pm 42$	$-64 \pm 35$	$32 \pm 14$	$470 \pm 371$	$400 \pm 149$
$\alpha$	$0.025 \pm 0.006$	$0.021 \pm 0.008$	$0.014 \pm 0.010$	$0.008 \pm 0.004$	$0.022 \pm 0.009$	$0.016 \pm 0.010$	$0.013 \pm 0.012$
$\beta \times 10^3$	$3.7 \pm 0.3$	$3.5 \pm 0.4$	$3.1 \pm 0.5$	$2.9 \pm 0.1$	$3.8 \pm 0.6$	$3.3 \pm 0.6$	$3.1 \pm 0.7$
$-\gamma$	$5.883 \pm 0.004$	$5.888 \pm 0.009$	$5.900 \pm 0.014$	$5.908 \pm 0.002$	$5.87 \pm 0.02$	$5.90 \pm 0.03$	$5.90 \pm 0.03$
$\delta$ , mbarn	$51.8 \pm 0.4$	$51.3 \pm 1.2$	$50 \pm 2$	$48.4 \pm 0.9$	$56 \pm 5$	$52 \pm 5$	$49 \pm 5$
$\bar{\alpha}$	$0.080 \pm 0.003$	$0.053 \pm 0.005$	$0.038 \pm 0.010$	$0.014 \pm 0.003$	$0.026 \pm 0.014$	$0.022 \pm 0.016$	$0.019 \pm 0.013$
$\bar{\beta} \times 10^3$	$9.1 \pm 0.3$	$6.2 \pm 0.4$	$4.9 \pm 0.7$	$3.18 \pm 0.12$	$4.0 \pm 0.9$	$3.8 \pm 0.1$	$3.6 \pm 0.8$
$-\bar{\gamma}$	$5.676 \pm 0.005$	$5.763 \pm 0.011$	$5.81 \pm 0.02$	$5.874 \pm 0.002$	$5.84 \pm 0.03$	$5.84 \pm 0.04$	$5.85 \pm 0.03$
$\bar{\delta}$ , mbarn	$127.3 \pm 1.6$	$96 \pm 3$	$81 \pm 7$	$63.0 \pm 1.2$	$74 \pm 10$	$75 \pm 14$	$72 \pm 9$
$\chi^2/\text{n.d.f.}$	423/306	186/237	113/153	87.3/122	62.2/87	33.1/58	31.4/52

TABLE X: Parameters for global simultaneous fitting by (3), (4), (10) and (11) of  $\sigma_{\text{tot}}^{pp}$ ,  $\sigma_{\text{tot}}^{\bar{p}p}$ ,  $\rho^{pp}$  and  $\rho^{\bar{p}p}$  energy dependencies.

$\sqrt{s}$ (TeV)	$\sqrt{s_{\min}}$						
	3	5	10	15	20	25	30
	$\sigma_{\text{tot}}^{pp}$ (mb)						
0.2	$51.34 \pm 3.80$	$51.53 \pm 5.33$	$51.55 \pm 7.12$	$52.37 \pm 1.93$	$52.66 \pm 7.82$	$53.69 \pm 9.60$	$51.7 \pm 10.6$
0.5	$59.87 \pm 5.30$	$60.25 \pm 7.34$	$60.32 \pm 9.69$	$61.68 \pm 2.84$	$62.1 \pm 10.3$	$62.7 \pm 12.0$	$60.6 \pm 13.7$
7	$91.5 \pm 11.4$	$93.3 \pm 15.8$	$95.0 \pm 20.8$	$99.49 \pm 7.10$	$97.6 \pm 20.7$	$97.7 \pm 23.1$	$96.4 \pm 27.7$
10	$96.3 \pm 12.4$	$98.5 \pm 17.2$	$100.6 \pm 22.8$	$105.73 \pm 7.89$	$103.2 \pm 22.5$	$103.3 \pm 25.0$	$102.2 \pm 30.2$
14	$101.0 \pm 13.4$	$103.5 \pm 18.6$	$106.1 \pm 24.7$	$111.84 \pm 8.68$	$108.5 \pm 24.3$	$108.8 \pm 27.0$	$107.8 \pm 32.6$
30	$111.8 \pm 15.8$	$115.1 \pm 22.1$	$119.0 \pm 29.5$	$126.5 \pm 10.7$	$120.9 \pm 28.6$	$121.6 \pm 31.9$	$121.2 \pm 38.7$
40	$115.9 \pm 16.8$	$119.6 \pm 23.5$	$124.0 \pm 31.5$	$132.3 \pm 11.5$	$125.7 \pm 30.3$	$126.7 \pm 33.9$	$126.4 \pm 41.2$
50	$119.1 \pm 17.6$	$123.2 \pm 24.6$	$128.0 \pm 33.0$	$136.9 \pm 12.1$	$129.4 \pm 31.6$	$130.6 \pm 35.4$	$130.6 \pm 43.2$
100	$129.3 \pm 20.2$	$134.4 \pm 28.3$	$140.8 \pm 38.2$	$151.7 \pm 14.3$	$141.2 \pm 36.1$	$143.2 \pm 40.7$	$143.8 \pm 49.7$
200	$139.6 \pm 22.9$	$145.8 \pm 32.2$	$154.0 \pm 43.8$	$167.2 \pm 16.8$	$152.3 \pm 40.9$	$156.3 \pm 46.3$	$157.7 \pm 56.8$
500	$153.2 \pm 26.7$	$161.1 \pm 37.9$	$172.3 \pm 52.0$	$189.0 \pm 20.4$	$169.4 \pm 47.6$	$174.1 \pm 54.5$	$176.7 \pm 67.1$
	$\sigma_{\text{tot}}^{\bar{p}p}$ (mb)						
0.546	$64.29 \pm 3.02$	$62.44 \pm 5.24$	$62.4 \pm 10.7$	$61.17 \pm 2.61$	$62.1 \pm 15.4$	$62.2 \pm 11.9$	$62.2 \pm 14.8$
1.8	$71.28 \pm 3.92$	$74.54 \pm 7.11$	$75.7 \pm 14.8$	$75.60 \pm 3.89$	$76.1 \pm 21.6$	$76.8 \pm 17.4$	$77.0 \pm 20.8$

TABLE XI: Predictions for  $\sigma_{\text{tot}}$  at various energies based on the simultaneous fits of energy dependence of proton-proton and proton-antiproton total cross-sections.

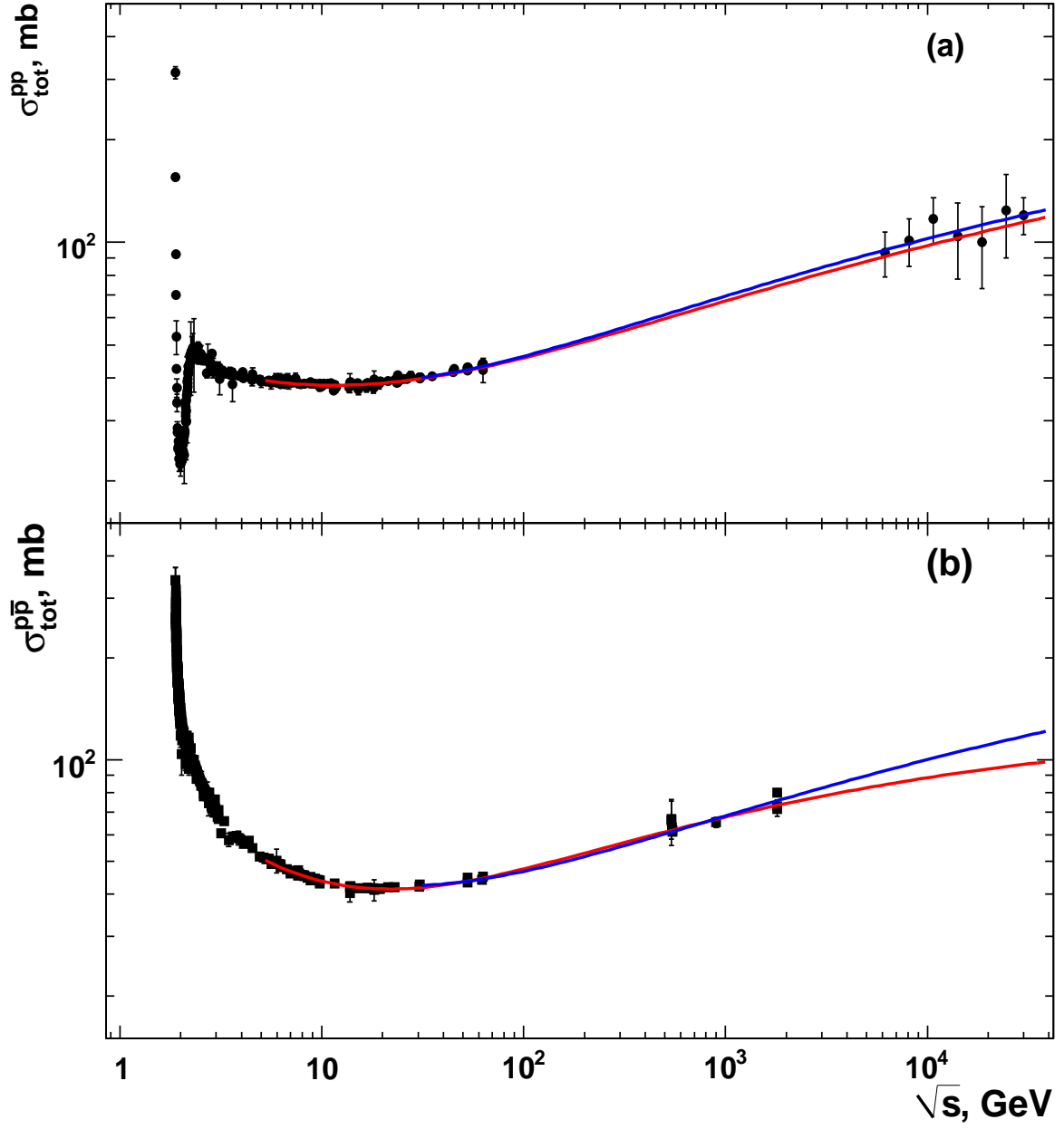


FIG. 1: (color online) Total cross-section energy dependence for proton-proton (a) and antiproton-proton (b) collisions. The red lines correspond to individual fits at  $\sqrt{s_{\text{min}}} = 5$ , the blue lines - at  $\sqrt{s_{\text{min}}} = 30$ . Experimental data are from [34].



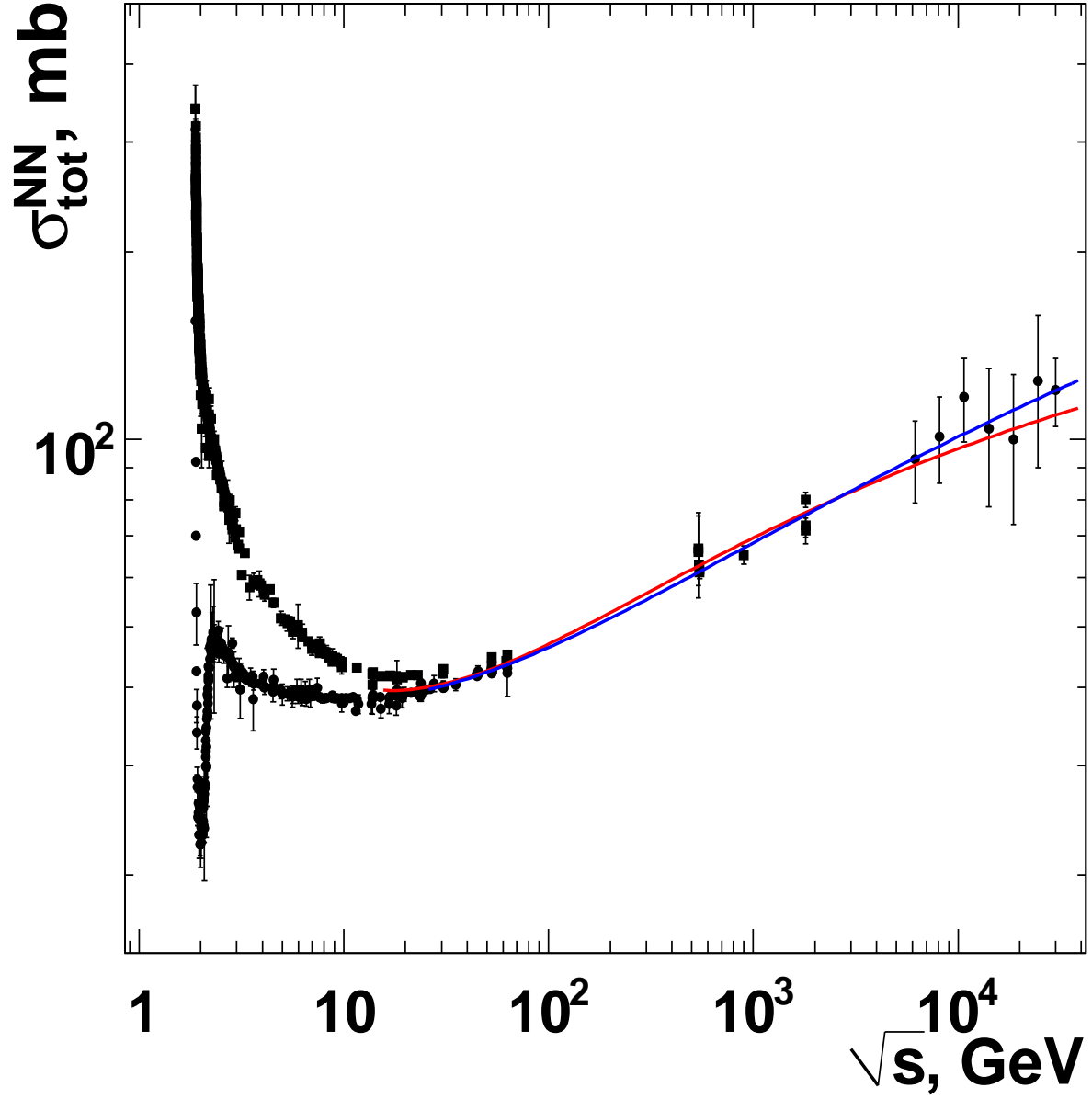


FIG. 2: (color online) Total cross-section energy dependence for nucleon-nucleon collisions. The red line corresponds to the fit at  $\sqrt{s_{\min}} = 15$ , the blue line - at  $\sqrt{s_{\min}} = 25$ . Experimental points are indicated as  $\bullet$  ( $\blacksquare$ ) for  $pp$  ( $p\bar{p}$ ). Experimental data are from [34].

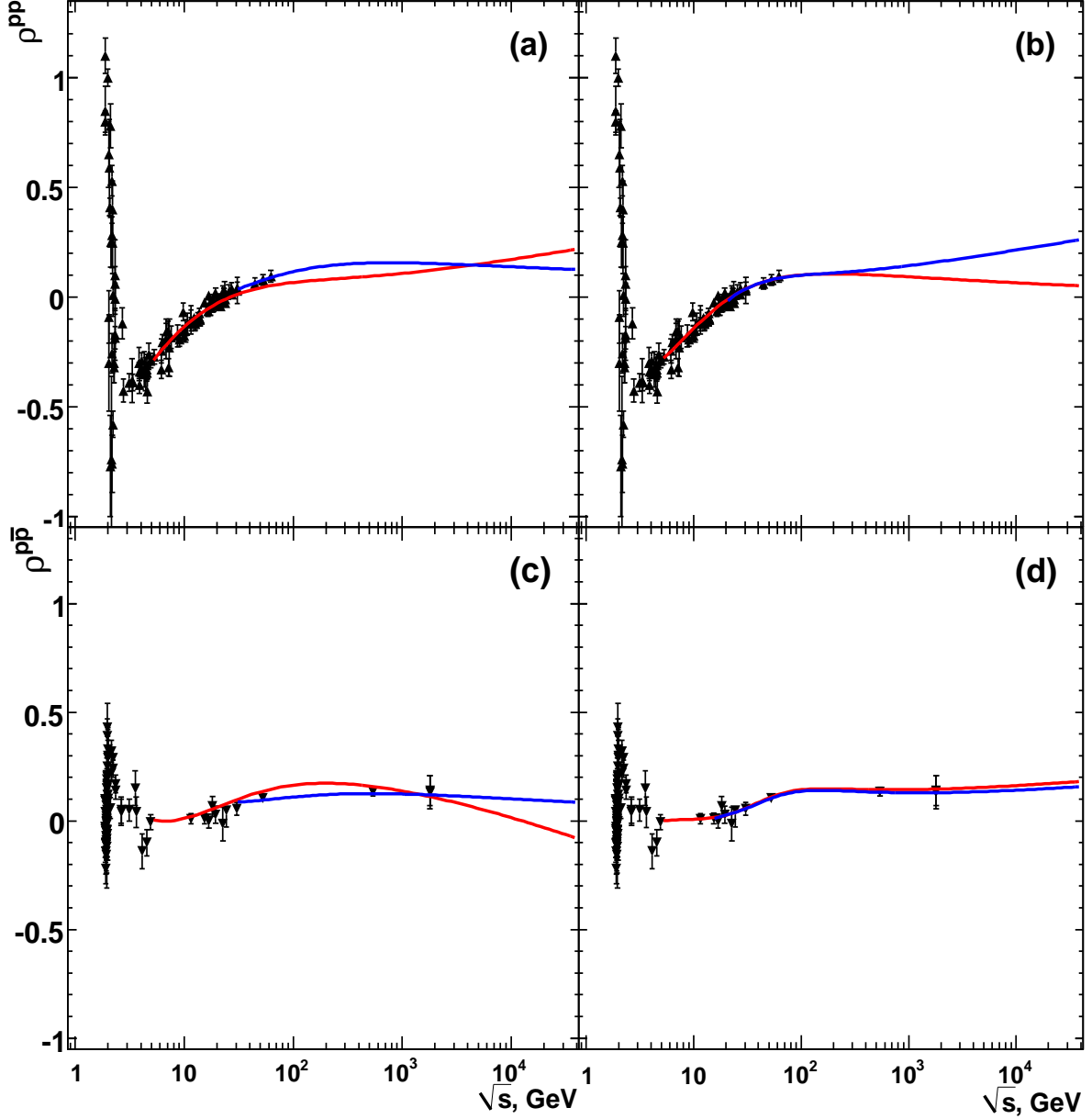


FIG. 3: (color online) The  $\rho$  parameter energy dependence for proton-proton (a,b) and antiproton-proton (c,d) collisions. Results obtained in the framework of i) approach for individual fit are shown on (a,c) and for approach ii) - on (b,d). The red lines correspond to the individual fits at  $\sqrt{s_{\min}} = 5$  for any approaches. Blue lines correspond to the individual fits at  $\sqrt{s_{\min}} = 30$  for i) approach (a,c) and for approximation curves obtained in the framework of ii) approach at  $\sqrt{s_{\min}} = 20$  (15) for  $pp$  ( $\bar{p}p$ ) respectively (b,d). Experimental data are from [34].

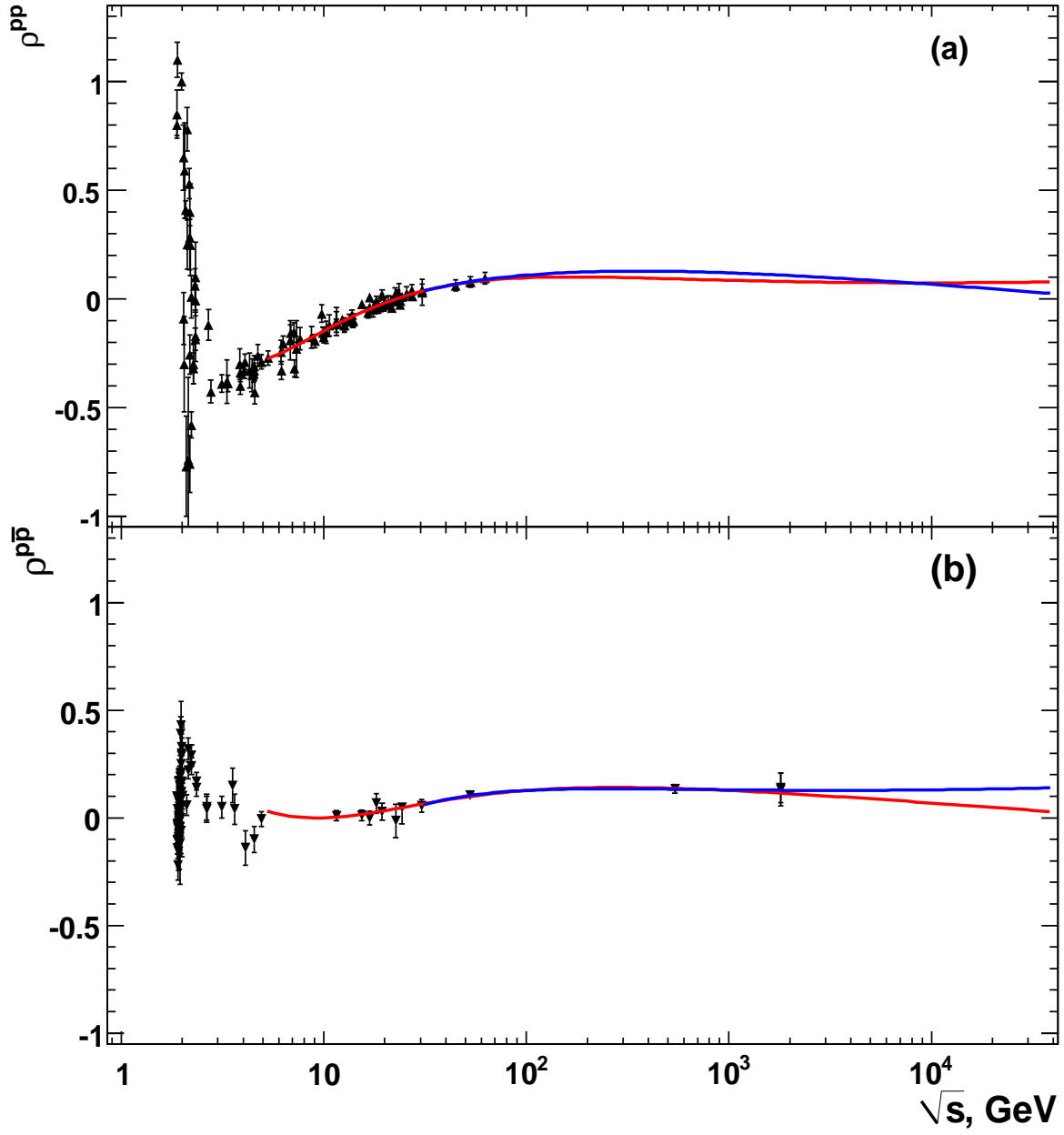


FIG. 4: (color online) The  $\rho$  parameter energy dependence for proton-proton (a) and antiproton-proton (b) collisions and results of simultaneous fits of these two parameters. The red line corresponds to the fit at  $\sqrt{s_{\min}} = 5$ , the blue line - at  $\sqrt{s_{\min}} = 30$ . Experimental data are from [34].

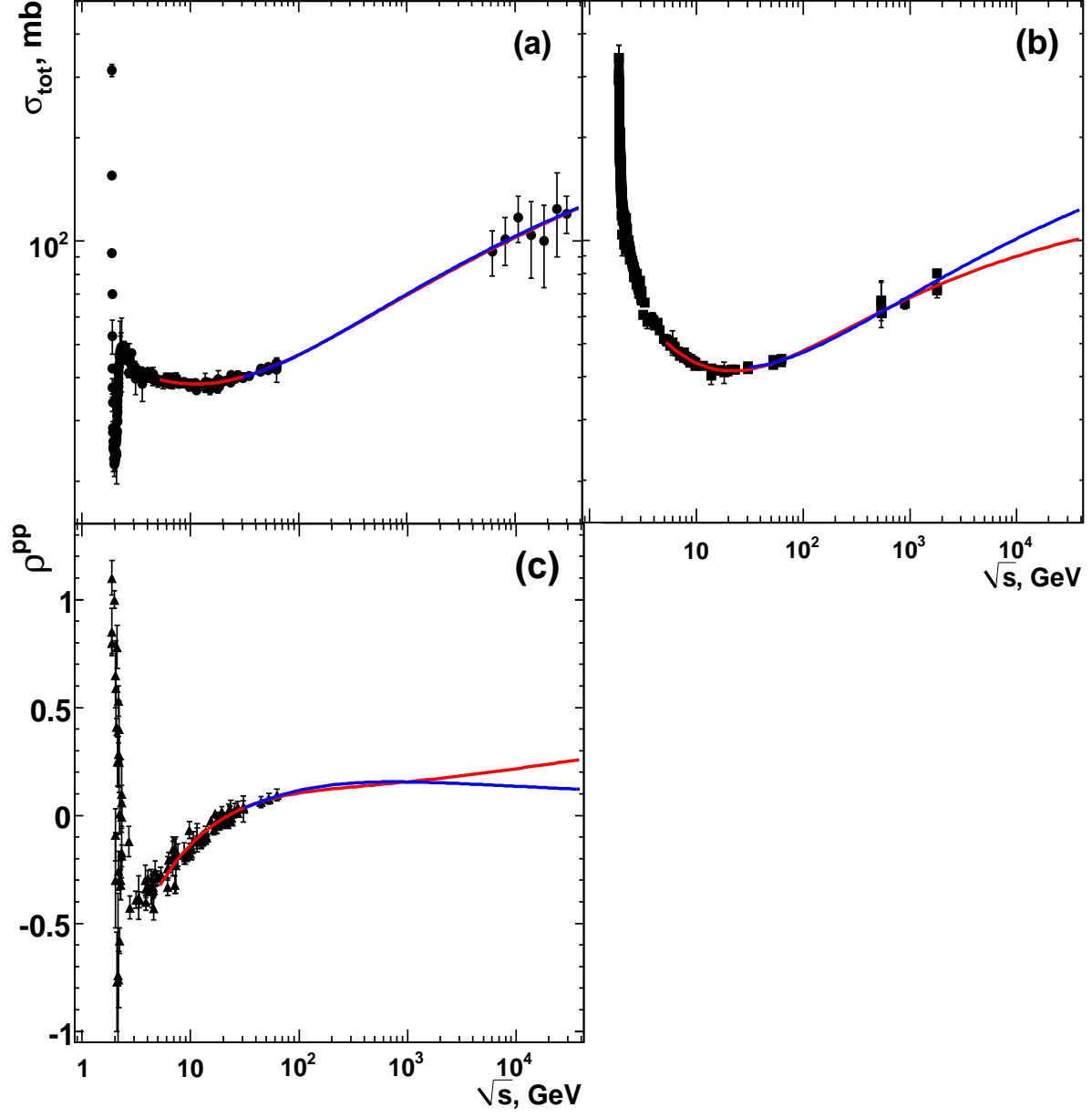


FIG. 5: (color online) The  $\sigma_{\text{tot}}$  energy dependence for proton-proton (a), antiproton-proton (b) collisions,  $\rho^{pp}$  parameter vs collision energy (c) and results of simultaneous fits of these parameters. The red line corresponds to the fit at  $\sqrt{s_{\text{min}}} = 5$ , the blue line - at  $\sqrt{s_{\text{min}}} = 30$ . Experimental data are from [34].

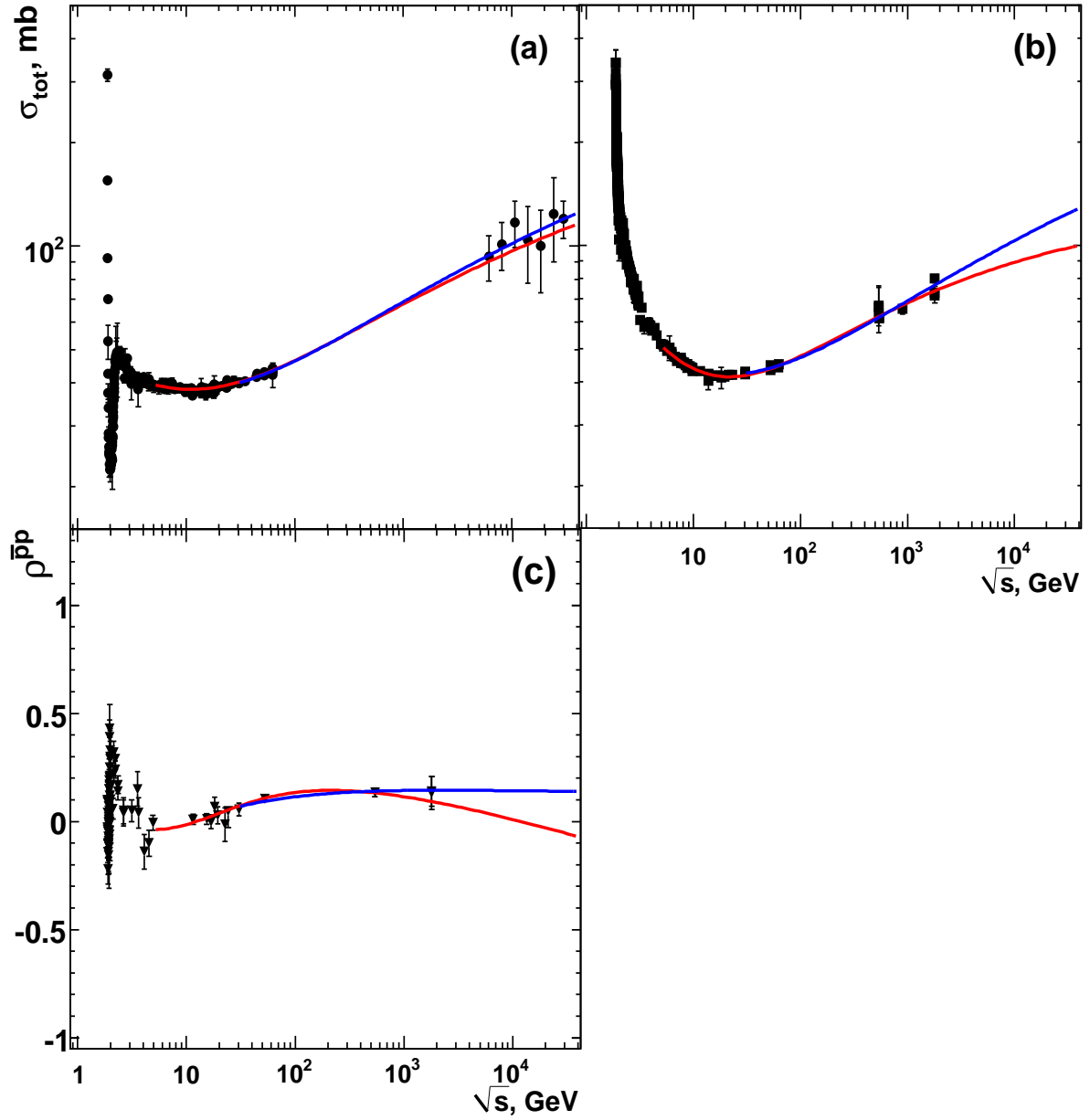


FIG. 6: (color online) The  $\sigma_{\text{tot}}$  energy dependence for proton-proton (a), antiproton-proton (b) collisions,  $\rho^{\bar{p}p}$  parameter vs collision energy (c) and results of simultaneous fits of these parameters. The red line corresponds to the fit at  $\sqrt{s_{\text{min}}} = 5$ , the blue line - at  $\sqrt{s_{\text{min}}} = 30$ . Experimental data are from [34].

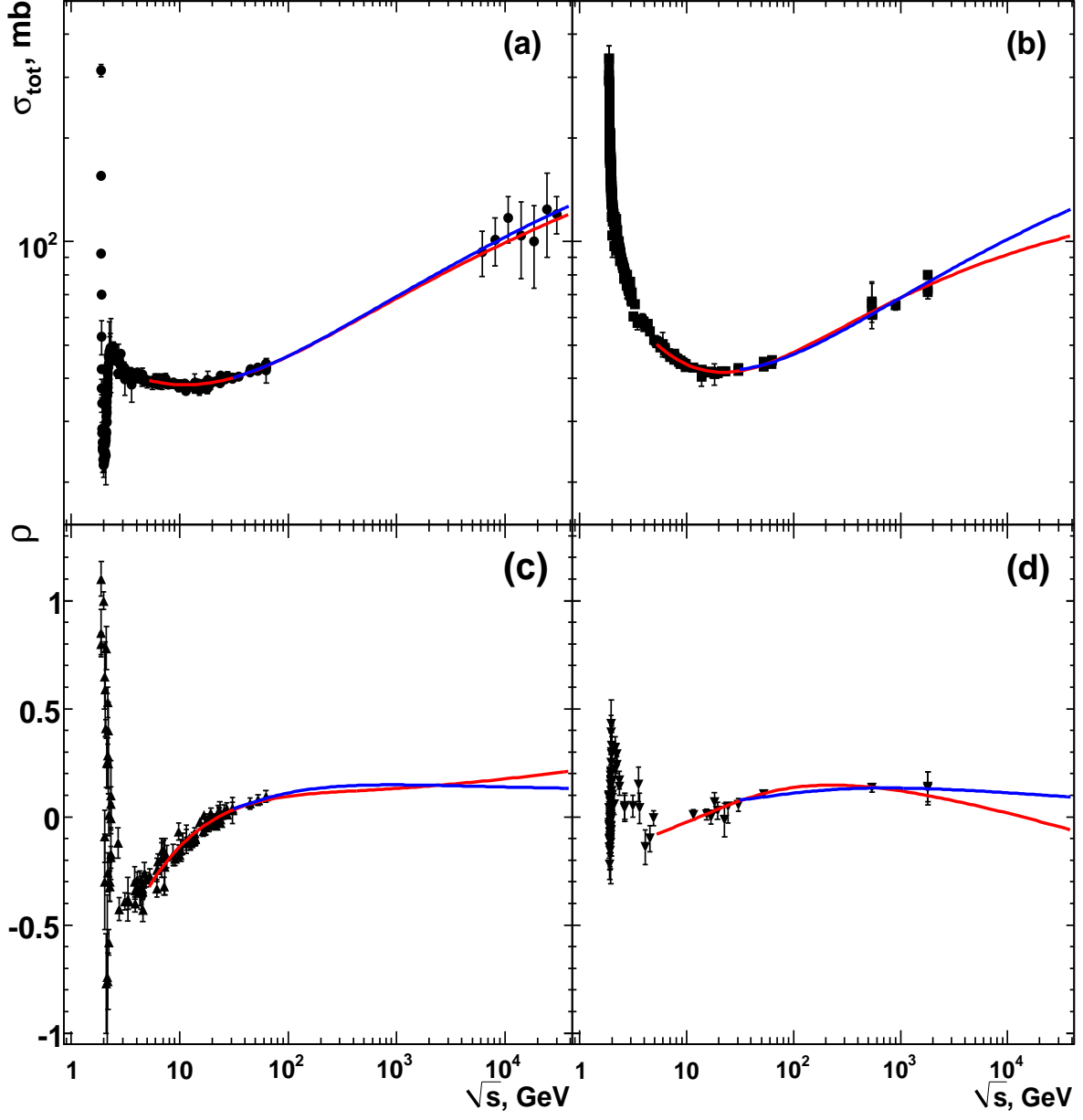


FIG. 7: (color online) The  $\sigma_{\text{tot}}$  energy dependence for proton-proton (a), antiproton-proton (b) collisions,  $\rho^{pp}$  (c),  $\rho^{\bar{p}p}$  (d) parameters vs collision energy and results of simultaneous fits of all four parameters. The red line corresponds to the fit at  $\sqrt{s_{\text{min}}} = 5$ , the blue line - at  $\sqrt{s_{\text{min}}} = 30$ . Experimental data are from [34].